© 2022. Published by The Company of Biologists Ltd | Journal of Cell Science (2022) 135, jcs260414. doi:10.1242/jcs.260414

CORRECTION

Correction: An evolutionarily distinct chaperone promotes 20S proteasome α-ring assembly in plants

Richard S. Marshall, David Gemperline, Fionn McLoughlin, Adam J. Book, Kay Hofmann and Richard D. Vierstra

This Correction replaces and updates a previous Correction to *J. Cell Sci.* (2020) **133**, jcs249862 (doi:10.1242/jcs.249862).

In Fig. S2, four bimolecular fluorescence microscopy (BiFC) confocal microscope images were inadvertently duplicated. These panels, which all contain only control background fluorescence, were not used to infer any positive interactions and the errors do not affect the results or conclusions of the paper.

The correct figure is shown below and the online supplementary material has been updated.

The authors apologise for these errors and any inconvenience caused.

Journal of Cell Science (2022) 135, jcs260414. doi:10.1242/jcs.260414

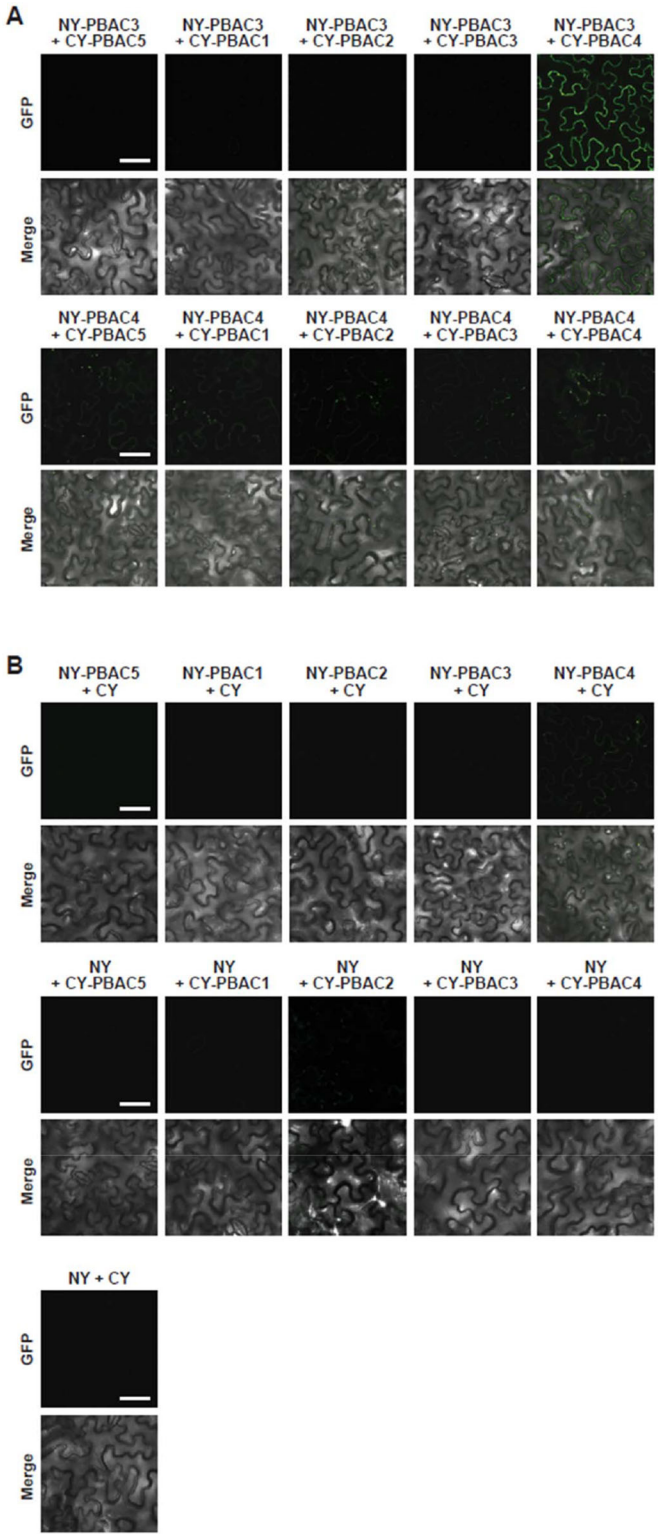

Fig. S2A (corrected). Control bimolecular fluorescence complementation (BiFC) assays involving PBAC1-5. (A) Pairwise expression of the PBAC3 and PBAC4 chaperones with themselves and PBAC1, PBAC2 and PBAC5 indicates that PBAC3 and PBAC4 interact in planta. (B) Pairwise expression of the PBAC1-5 chaperones fused to the N-terminal (NY) and C-terminal (CY) halves of YFP by themselves indicate that only the NY-PBAC4 construct produces a fluorescence signal due to auto-activation. *Nicotiana benthamiana* leaf epidermal cells were co-infiltrated with the indicated plasmid combinations, and fluorescence signals were detected by confocal fluorescence microscopy 36 h after infiltration. Shown are the fluorescence images alone or merged with their companion bright field images. Scale bar=20 µm.

Journal of Cell Science (2022) 135, jcs260414. doi:10.1242/jcs.260414

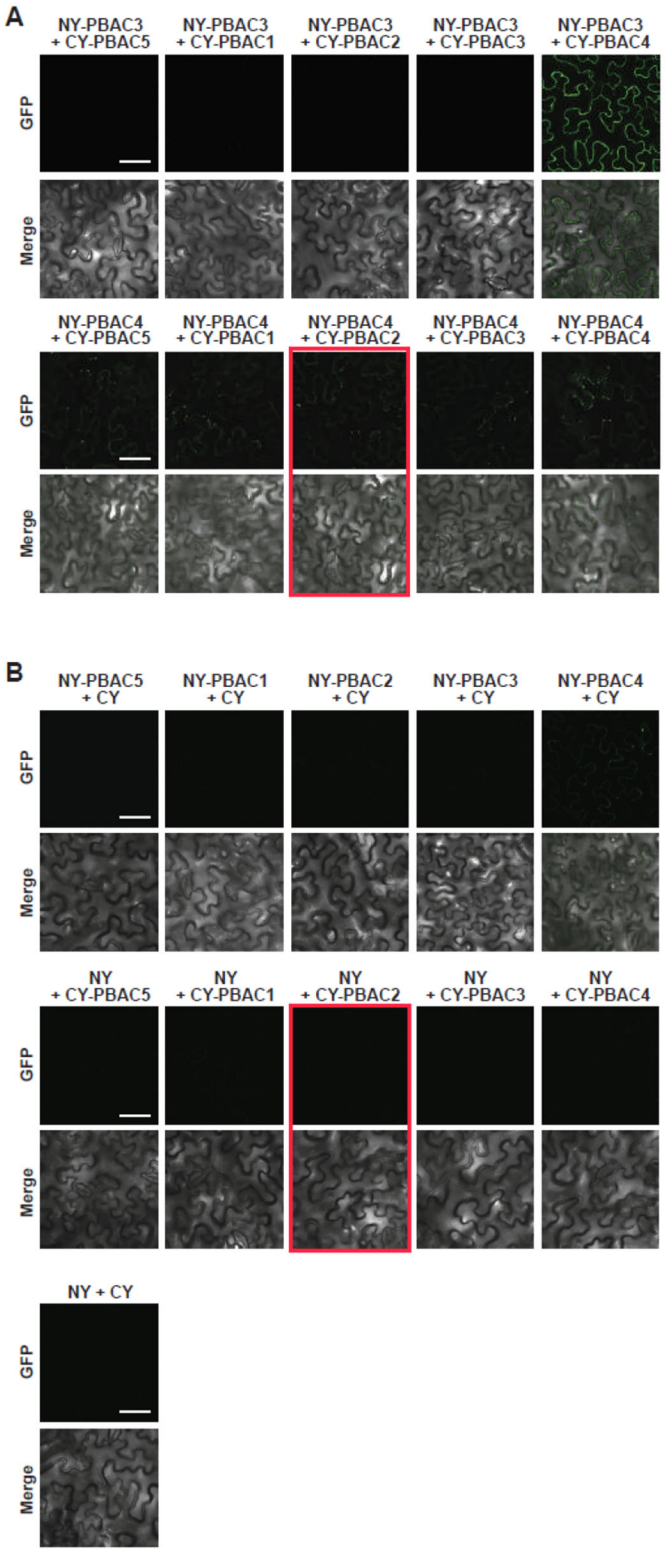

Fig. S2A (original). Control bimolecular fluorescence complementation (BiFC) assays involving PBAC1-5. (A) Pairwise expression of the PBAC3 and PBAC4 chaperones with themselves and PBAC1, PBAC2 and PBAC5 indicates that PBAC3 and PBAC4 interact in planta. (B) Pairwise expression of the PBAC1-5 chaperones fused to the N-terminal (NY) and C-terminal (CY) halves of YFP by themselves indicate that only the NY-PBAC4 construct produces a fluorescence signal due to auto-activation. *Nicotiana benthamiana* leaf epidermal cells were co-infiltrated with the indicated plasmid combinations, and fluorescence signals were detected by confocal fluorescence microscopy 36 h after infiltration. Shown are the fluorescence images alone or merged with their companion bright field images. Scale bar=20 µm. Duplicated panels are indicated in red boxes.

© 2020. Published by The Company of Biologists Ltd | Journal of Cell Science (2020) 133, jcs249862. doi:10.1242/jcs.249862

RESEARCH ARTICLE

An evolutionarily distinct chaperone promotes 20S proteasome α-ring assembly in plants

Richard S. Marshall[1,2], David C. Gemperline[2], Fionn McLoughlin[1], Adam J. Book[2], Kay Hofmann[3] and Richard D. Vierstra[1,2,*]

ABSTRACT

The core protease (CP) subcomplex of the 26S proteasome houses the proteolytic active sites and assumes a barrel shape comprised of four co-axially stacked heptameric rings formed by structurally related α- and β-subunits. CP biogenesis typically begins with the assembly of the α-ring, which then provides a template for β-subunit integration. In eukaryotes, α-ring assembly is partially mediated by two hetero-dimeric chaperones, termed Pba1–Pba2 (Add66) and Pba3–Pba4 (also known as Irc25–Poc4) in yeast. Pba1–Pba2 initially promotes orderly recruitment of the α-subunits through interactions between their C-terminal HbYX or HbF motifs and pockets at the α_5–α_6 and α_6–α_7 interfaces. Here, we identified PBAC5 as a fifth α-ring assembly chaperone in *Arabidopsis* that directly binds the Pba1 homolog PBAC1 to form a trimeric PBAC5–PBAC1–PBAC2 complex. PBAC5 harbors a HbYX motif that docks with a pocket between the α_4 and α_5 subunits during α-ring construction. *Arabidopsis* lacking PBAC5, PBAC1 and/or PBAC2 are hypersensitive to proteotoxic, salt and osmotic stresses, and display proteasome assembly defects. Remarkably, whereas PBAC5 is evolutionarily conserved among plants, sequence relatives are also dispersed within other kingdoms, including a scattered array of fungal, metazoan and oomycete species.

KEY WORDS: *Arabidopsis*, Chaperone, Core protease, Degradation, Evolution, Proteasome, Proteolysis, Proteostasis, Regulatory particle, Ubiquitin

INTRODUCTION

Selective protein degradation is crucial for almost every aspect of cellular physiology. While the degradation of mis-translated, mis-folded, damaged or otherwise malfunctioning proteins is essential for maintaining intracellular proteostasis (Marshall and Vierstra, 2019; Pohl and Dikic, 2019), the timely removal of regulatory proteins is required for most, if not all, cellular processes, including the cell cycle, signal transduction, neuronal signaling, transcription, DNA repair and translation (Ahuja et al., 2017; Brinkmann et al., 2015; Ramachandran et al., 2018). Consequently, disruptions in selective proteolysis often lead to an array of pathologies, including hypersensitivity to proteotoxic stress, cancer, neurodegeneration, immune-related disorders and accelerated ageing (Higuchi-Sanabria et al., 2018; Pilla et al., 2017; Rape, 2018).

A main proteolytic route in eukaryotes is the ubiquitin–proteasome system (UPS) (Finley et al., 2012; Marshall and Vierstra, 2019). Here, substrates are targeted by the selective attachment of polyubiquitin chains with appropriate topologies by a myriad of substrate-specific E3 ubiquitin–protein ligases (Zheng and Shabek, 2017). Breakdown of the ubiquitylated proteins is then directed by the 26S proteasome, which recognizes the polyubiquitin, unfolds the modified protein, releases the ubiquitin moieties for re-use, and cleaves the linear polypeptide into short fragments using relatively non-specific peptidase activities (Finley and Prado, 2020; Greene et al., 2020; Marshall and Vierstra, 2019).

The 26S proteasome is composed of two stable and functionally distinct subcomplexes; the 20S core protease (CP) that provides the peptidase activities, capped at one or both ends by the 19S regulatory particle (RP) that captures and prepares appropriate substrates for breakdown (Bhattacharyya et al., 2014; Greene et al., 2020). The CP assumes a barrel shape generated by four stacked heptameric rings that form upon the association of seven α- and β-subunits in a C_2-symmetric αββα configuration. Whereas eukaryotes employ structurally related but distinct α- and β-subunit isoforms to generate the barrel, their archaeal and bacterial progenitors often use single α- and β-subunit proteins to assemble homo-heptameric CP rings (Gille et al., 2003; Majumder and Baumeister, 2019). Upon assembly, a central chamber is created at the interface between the β-rings; in eukaryotes the β_1, β_2, and β_5 subunits provide six catalytic sites within this lumen (Arendt and Hochstrasser, 1997; Heinemeyer et al., 1997), whereas in archaea and bacteria, all 14 β-subunits are presumably active (Majumder et al., 2019; Seemüller et al., 1995).

Atop each β-subunit ring sits the α-subunit ring, which creates two narrow axial pores that are gated by a short N-terminal sequence extending from several α-subunits (Groll et al., 2000; Köhler et al., 2001; Rabl et al., 2008). Gate opening is normally triggered by docking of the CP to various proteasome regulators (Majumder and Baumeister, 2019), the most prominent being the RP. These regulators, or their subunits, often possess an extended C-terminal HbYX or HbF motif (Hb, hydrophobic residue; Y, tyrosine; F, phenylalanine; and X, any amino acid) that inserts into a shallow pocket formed at the interface between adjacent α-subunits (Rabl et al., 2008; Smith et al., 2007; Tian et al., 2011). Through this distinctive and stable architecture, the CP acts as a self-compartmentalized protease that degrades polypeptides that are deliberately imported into the β-ring chamber.

Assembly of a complete 26S proteasome from its 32 or more distinct constituents is a highly complicated process that requires a suite of dedicated chaperones and maturation factors for precise construction of both the CP and RP (Howell et al., 2017; Marshall and Vierstra, 2019; Rousseau and Bertolotti, 2018). As the eukaryotic CP requires the orderly recruitment of the α- and

[1]Department of Biology, Washington University in St. Louis, 1 Brookings Drive, St. Louis, MO 63130, USA. [2]Department of Genetics, University of Wisconsin, 425 Henry Mall, Madison, WI 53706, USA. [3]Institute for Genetics, University of Cologne, Zülpicher Straße 47a, 50674 Cologne, Germany.

*Author for correspondence (rdvierstra@wustl.edu)

R.S.M., 0000-0002-6844-1078; F.M., 0000-0002-2430-5074; A.J.B., 0000-0002-0253-9494; K.H., 0000-0002-2289-9083; R.D.V., 0000-0003-0210-3516

Handling Editor: John Heath
Received 8 June 2020; Accepted 21 September 2020

Journal of Cell Science (2020) 133, jcs249862. doi:10.1242/jcs.249862

β-subunits, its correct formation is particularly challenging to maintenance of a healthy proteasome pool devoid of dysfunctional products. CP assembly typically begins with construction of the individual α-rings, followed by β-subunit incorporation (Hirano et al., 2008; Li et al., 2007), though α-ring-independent assembly pathways have also been reported (Hammack et al., 2020; Panfair et al., 2015). Creation of the eukaryotic α-ring is controlled by a hetero-dimeric chaperone termed Pba1–Pba2 (also known as Pba1–Add66) in the budding yeast *Saccharomyces cerevisiae* and PAC1–PAC2 in mammals (also known as PSMG1–PSMG2) that provides a template onto which several α-subunits correctly associate, namely α_5, α_6 and α_7 (Hirano et al., 2005; Kock et al., 2015; Stadtmueller et al., 2012; Wani et al., 2015). Binding of Pba1 and Pba2 to the cognate α-subunit pairs is stabilized through interactions between their C-terminal HbYX motifs (HbF in mammalian PAC2) and pockets at the α_5–α_6 and α_6–α_7 interfaces, respectively, thus placing the α_5–α_6–α_7 trimer in correct register (Kusmierczyk et al., 2011; Wu et al., 2018). Although still viable, yeast lacking Pba1 or Pba2 accumulate immature CP species containing structurally unstable α-rings, from which α_5 and α_6 readily dissociate (Wani et al., 2015), whereas comparable mammalian mutants accumulate fewer α-rings (Hirano et al., 2005).

How the α_1, α_2, α_3 and α_4 subunits then integrate is unclear, but the hetero-dimeric Pba3–Pba4 chaperone in yeast (also known as Irc25–Poc4) and the PAC3–PAC4 chaperone in mammals (also termed PSMG3–PSMG4) appear critical for correct stoichiometry of the α_3 and α_4 subunits (Kusmierczyk et al., 2008; Padmanabhan et al., 2016; Takagi et al., 2014), and integration of the α_1 subunit appears rate limiting (Howell et al., 2019). The Pba1–Pba2 and Pba3–Pba4 pairs also prevent premature association of CP assembly intermediates with the RP or other activating factors, in some cases by outcompeting HbYX-containing RP subunits such as Rpt5 for CP binding until the CP rings mature (Kock et al., 2015; Stadtmueller et al., 2012; Wani et al., 2015).

Upon completion, the α-ring provides a platform for β-ring assembly, the orderly recruitment of which requires the maturation factor Ump1 (POMP in humans) (Gemperline et al., 2019; Ramos et al., 1998) and the N-terminal propeptides present in several β-subunits (Chen and Hochstrasser, 1996; Hirano et al., 2008; Li et al., 2007). A transient 15S 'half-proteasome' emerges, which ultimately dimerizes to generate the mature 20S CP, possibly with the help of the capping factor PA200 (also known as PSME4 in humans; Blm10 in yeast) which also harbors a HbYX motif (Guan et al., 2020). Assembly of the mature CP is rate limited by final integration of the β_7 subunit. This association promotes half-proteasome dimerization followed by auto-catalytic removal of the N-terminal propeptides in β_1, β_2 and β_5, which then exposes their catalytic N-terminal threonine residues.

Although our understanding of CP assembly in yeast and mammals is reasonably well developed, the pathway(s) for constructing the plant CP remain unclear. Our prior proteomic analyses of *Arabidopsis* proteasomes led to the discovery of likely plant orthologs of yeast Pba1–Pba4 and Ump1, strongly suggesting that CP assembly follows the same path (Gemperline et al., 2019; Wang et al., 2019). Surprisingly, whereas yeast *Δump1* mutants are viable, *Arabidopsis* mutants null for its two functional orthologs are lethal due to defects in gametogenesis and/or seed development, implying that subtle differences in CP assembly exist. *Arabidopsis* mutants missing the dominant UMP1a isoform (At1g67250) are viable, but they are hypersensitive to proteotoxic stress and have compromised 26S proteasome assembly, consistent with UMP1 having CP maturation activity (Gemperline et al., 2019).

Besides the above chaperones, our mass spectrometric (MS) analyses also identified a fifth possible chaperone associated with the *Arabidopsis* CP, whose amino acid sequence is distantly related to PBAC1 and PBAC2, but includes the signature HbYX motif (Gemperline et al., 2019). Here we show that this protein, designated as PROTEASOME BIOGENESIS-ASSOCIATED CHAPERONE 5 (PBAC5; At3g07640), assembles with PBAC1 and PBAC2 to form a trimeric complex that can replace the Pba1–Pba2 dimer in yeast α-ring assembly. *Arabidopsis pbac5* mutants, like those missing PBAC1 and PBAC2, have CP assembly defects, elevated levels of ubiquitylated proteins and a hypersensitivity to proteotoxic stress, consistent with proteasome insufficiency. Remarkably, while PBAC5 orthologs could be found throughout the plant kingdom, they were also evident in a scattered array of fungal, metazoan and oomycete species. Taken together, the observations reported in this study extend our appreciation of proteasome assembly in plants, and for the first time describe a fifth chaperone required for efficient CP construction.

RESULTS

Identification of an uncharacterized plant proteasome-interacting protein

Our prior MS characterizations of *Arabidopsis* 26S proteasomes, affinity-purified through FLAG-tagged versions of the CP subunit PAG1 (α_7) or the RP subunit RPT4, identified all predicted core 26S subunits, plus an array of interacting proteins that included homologs of most yeast and mammalian CP and RP assembly chaperones (Book et al., 2010; Gemperline et al., 2019). One notable exception was an uncharacterized protein (PBAC5) of 241 amino acids found at high levels in preparations enriched in the CP alone, but not in the RP or the entire 26S particle. Because PBAC5 was most abundant in samples generated from seedlings treated with the proteasome inhibitor MG132, which also encourages proteasome synthesis (Gemperline et al., 2019), we speculated that it participates in CP assembly and not in the functions of the mature CP or 26S holocomplex.

Position-specific iterative basic local alignment search tool (PSI-BLAST) searches identified obvious orthologs of *Arabidopsis* PBAC5 throughout the plant kingdom, with 80–90% amino acid sequence identity in close relatives such as *Arabidopsis lyrata* and *Brassica rapa*, but just 30–35% identity in monocots such as rice and maize, and 20% identity in the moss *Physcomitrella patens* (Fig. S1A). By contrast, similar searches failed to find human or yeast relatives. Surprisingly, comparisons of hidden Markov models (HMM) constructed from different protein families (Söding, 2005) revealed a significant similarity (P<0.01) between the PBAC5 family and the PBAC1 and PBAC2 families (25% and 20% identity, respectively, in *Arabidopsis*), which by phylogenetic analyses clustered outside the plant PBAC5 family (Fig. 1A; Fig. S1B). This relationship was further supported by the presence of a C-terminal Leu-Tyr-Gly sequence analogous to the HbYX motif present in Pba1/PAC1/PBAC1, Pba2/PBAC2 and other CP α-ring-interacting proteins (Fig. 1B; Fig. S1A; Guan et al., 2020; Kusmierczyk et al., 2011; Rabl et al., 2008; Tian et al., 2011). Given this sequence homology and affinity for the CP, we predicted that PBAC5 participates in CP α-ring assembly.

Under the assumption that proteasome assembly chaperones should be co-ordinately expressed to meet proteolytic demand, we attempted to support this relationship between *Arabidopsis* PBAC5, PBAC1 and PBAC2 by gene co-expression analysis based on the transcript patterns available within the Transcriptome Variation Analysis database (www.travadb.org/; Klepikova et al., 2016).

Journal of Cell Science (2020) 133, jcs249862. doi:10.1242/jcs.249862

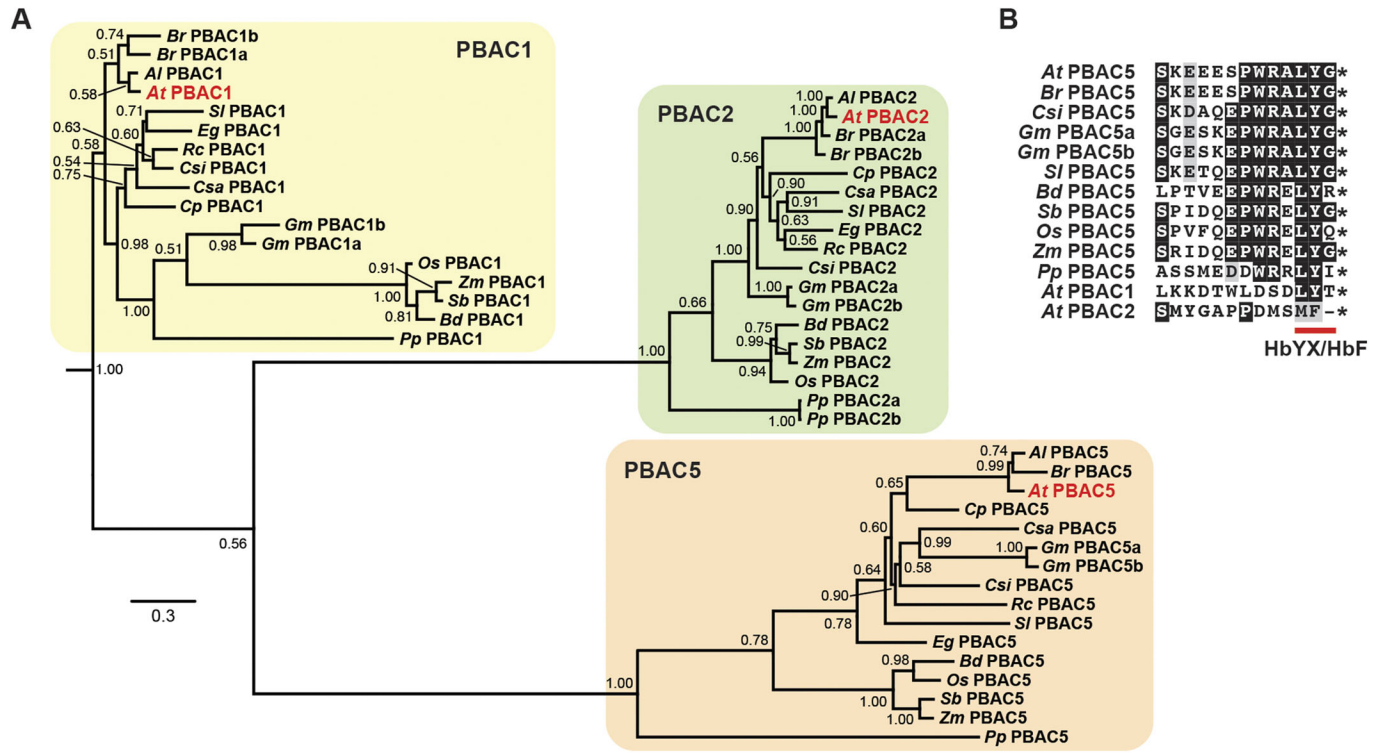

Fig. 1. Phylogenetic analysis of *Arabidopsis* PBAC5 reveals a novel family of proteasome chaperones. (A) Phylogenetic analysis comparing plant PBAC5 sequences with those of PBAC1 and PBAC2. The full-length amino acid sequences were subjected to Bayesian phylogenetic analysis, and the resulting consensus tree displayed using FigTree. All nodes have a bootstrap value of 1.00 unless otherwise indicated. The scale bar represents substitutions per site. (B) Sequence alignment of the C-terminal region of plant PBAC5 proteins, plus *Arabidopsis* PBAC1 and PBAC2. Identical (50% threshold) and similar amino acids are shown with black and gray backgrounds, respectively. The HbYX motif is underlined. Full alignments are in Fig. S1A. Species abbreviations are in the Materials and Methods.

Unfortunately, a common theme was not detected, even among chaperones that should work together (e.g. PBAC1–PBAC2 and PBAC3–PBAC4; Fig. S1C). *PBAC5* expression was highest in seeds, shoots, seedling meristems and, in contrast to the other CP chaperones, in senescing silique pods (Fig. S1C).

PBAC5 interacts with CP α-subunits and the PBAC1 assembly chaperone

To confirm the interaction between PBAC5 and proteasomes, and to identify the subcomplex to which it binds, we generated a transgenic *Arabidopsis* line overexpressing HA-tagged PBAC5 for co-immunoprecipitation studies with seedlings treated with or without MG132 (Gemperline et al., 2019). Here, the fully functional *HA–PBAC5* transgene was introduced into the *pbac5-3* null mutant (see below) and expressed with the tag appended in-frame to the N-terminus of PBAC5, to avoid interference with the HbYX motif. Immunoblotting the immunoprecipitates from untreated seedlings easily detected HA–PBAC5 in association with the CP α-ring, based on co-enrichment with the CP α-subunits PAC1 (α_3) and PAG1 (α_7). However, no association was seen between HA–PBAC5 and the PBA1 (β_1) or PBF1 (β_6) subunits from the β-ring, or any of the seven RP subunits examined, despite their easy detection in the input samples (Fig. 2A).

Notably, the interactions between HA–PBAC5 and PAC1 (α_3) and PAG1 (α_7) were enhanced upon pretreating *Arabidopsis* with MG132 (Fig. 2A). We also detected unprocessed PBA1 (β_1) in these HA–PBAC5 immunoprecipitates, which not only confirmed the efficacy of the MG132 on inhibiting proteasome maturation (Book et al., 2010; Chen and Hochstrasser, 1996), but also demonstrated that PBAC5 preferentially associated with CP assembly intermediates. As compared to the inputs, which contained both unprocessed and mature forms of PBA1, only the unprocessed form was evident in the HA–PBAC5 immunoprecipitates (Fig. 2A).

Based on the observations that yeast and mammalian Pba1/PAC1 and Pba2/PAC2 assemble into hetero-dimers (Hirano et al., 2005; Le Tallec et al., 2007; Stadtmueller et al., 2012), and our observations that *Arabidopsis* PBAC5 co-enriched with PBAC1 and PBAC2 in affinity-purified proteasomes (Gemperline et al., 2019), we predicted that PBAC5 interacts with PBAC1 and/or PBAC2. As a first test, we assayed each combination using yeast two-hybrid (Y2H) assays. As shown in Fig. 2C, interactions were clearly evident for the PBAC1–PBAC2 and PBAC3–PBAC4 pairs, consistent with the known dimerization of their yeast and mammalian counterparts (Hirano et al., 2006; Kusmierczyk et al., 2008; Le Tallec et al., 2007; Takagi et al., 2014; Yashiroda et al., 2008). By contrast, PBAC5 showed a clear interaction only with PBAC1, and not with any of the other PBAC chaperones.

We next tested the interactions *in planta* with bimolecular fluorescence complementation (BiFC) assays using tobacco (*Nicotiana benthamiana*) leaf cells, which expressed the chaperones as N-terminal fusions with either the N- or C-terminal halves of yellow fluorescent protein (YFP). Again, reconstitution of cellular fluorescence was seen when the PBAC1–PBAC2 and PBAC3–PBAC4 pairs were co-expressed, but a similar signal was evident only when PBAC5 was co-expressed with PBAC1 (Fig. 2B; Fig. S2). Taken together, our data implies that *Arabidopsis* PBAC5 forms a hetero-trimeric complex with the proteasome assembly chaperones PBAC1 and PBAC2 in a PBAC5–PBAC1–PBAC2 orientation, and that this complex primarily interacts with the CP α-ring.

Journal of Cell Science (2020) 133, jcs249862. doi:10.1242/jcs.249862

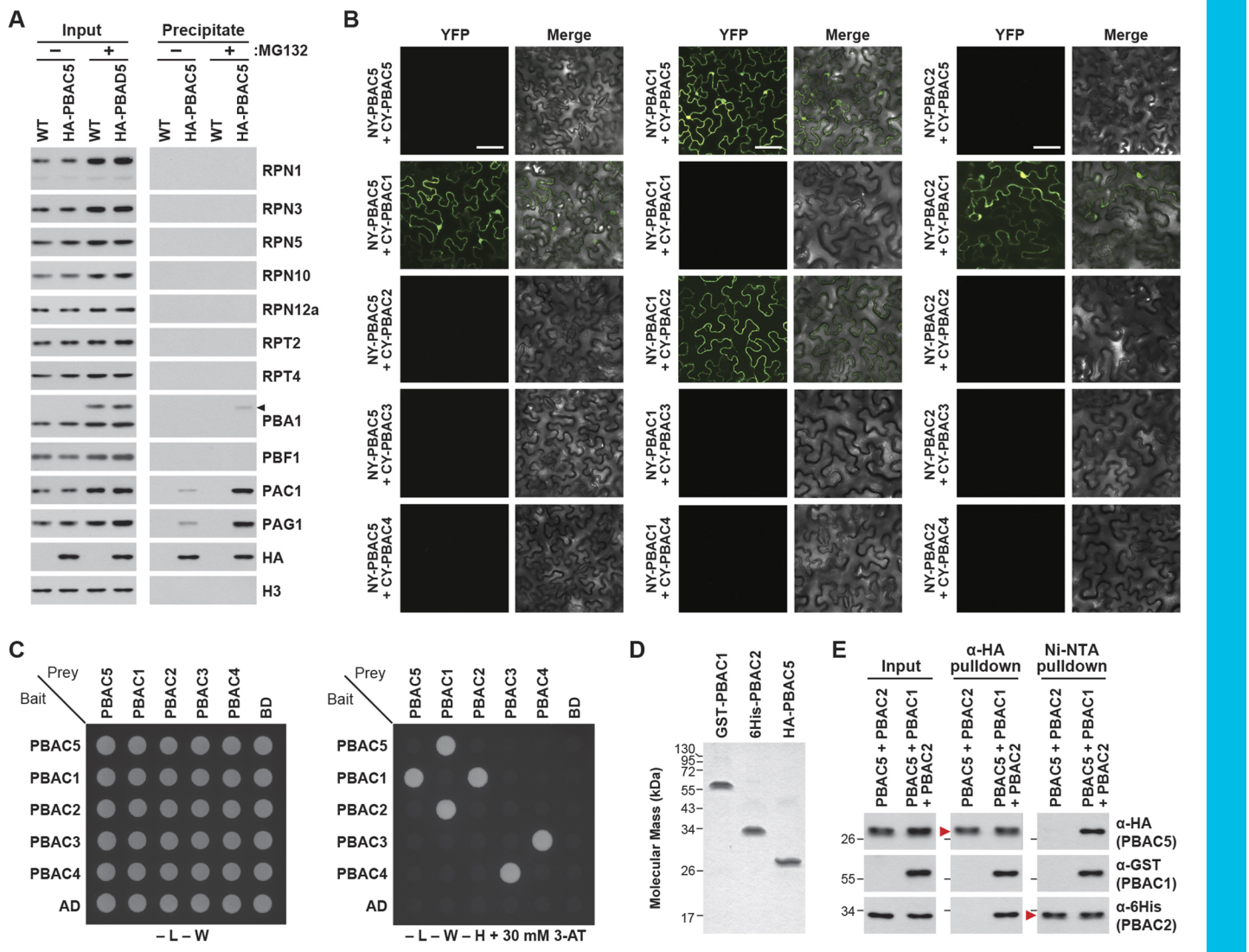

Fig. 2. PBAC5 interacts with the 26S proteasome CP α-ring and with PBAC1 and PBAC2. (A) Co-immunoprecipitation of *Arabidopsis* CP subunits with HA-tagged PBAC5. Protein extracts from seedlings treated with DMSO (control, –) or 50 µM MG132 (+) were immunoprecipitated with anti-HA agarose beads. The input and elution (precipitate) fractions were then immunoblotted with the indicated antibodies. Immunodetection of histone H3 was included as a negative control. Numbers on the left represent molecular mass markers in kDa. The arrowhead locates unprocessed PBA1. (B) BiFC assays demonstrating interactions between PBAC5 and PBAC1, and PBAC1 and PBAC2, *in planta*. The indicated combinations of protein fusions to the N-terminal (NY) and C-terminal (CY) halves of EYFP were transiently co-expressed in *N. benthamiana* leaf cells, and reconstituted fluorescence (YFP) was imaged using confocal microscopy. Control interactions are in Fig. S2. Scale bars: 20 µm. (C) Y2H assays confirming the interactions between PBAC5 and PBAC1, PBAC1 and PBAC2, and PBAC3 and PBAC4. Coding regions fused to the Gal4 activation domain or DNA-binding domain (AD and BD, respectively) were co-expressed in yeast strain MaV203. Colonies were grown on control (–L –W) or selective (–L –W –H +3-AT) medium. (D) Purity of GST–PBAC1, 6His–PBAC2 and HA–PBAC5 used for *in vitro* pulldown assays in E. The recombinant proteins (2 µg) were subjected to SDS–PAGE and stained with Coomassie Brilliant Blue. (E) *In vitro* pulldown assays confirm that PBAC1 tethers PBAC5 to PBAC2. Equal amounts (1 µg) of purified proteins were mixed and pulled down with anti-HA agarose beads or Ni-NTA agarose beads. Input and bound proteins were detected by immunoblotting with the indicated antibodies. The red arrowheads identify the protein directly immunoprecipitated from each mixture.

The *Arabidopsis* PBAC5–PBAC1–PBAC2 complex can functionally replace the yeast Pba1–Pba2 assembly chaperone

To help confirm that the PBAC5–PBAC1–PBAC2 complex is involved in proteasome assembly, we attempted to rescue yeast mutants missing Pba1 and Pba2 with their potential *Arabidopsis* orthologs. By themselves, neither the *Δpba1* nor the *Δpba2* strains (nor the *Δpba1 Δpba2* double mutant) show obvious growth defects (Kusmierczyk et al., 2011; Li et al., 2007). However, these mutants become sensitive to proteotoxic stress when proteasome function is further compromised by secondary mutations, such as the *doa5-1* allele impairing the CP α_5 subunit Doa5 (also known as Pup2; Chen and Hochstrasser, 1996), which can be seen by suppressed colony growth at low concentrations of the amino acid analog canavanine (Kusmierczyk et al., 2011). Although the *doa5-1 Δpba1* and *doa5-1 Δpba2* mutants were hypersensitive to canavanine, re-introduction of functional Pba1 or Pba2 from yeast, respectively, rescued this growth suppression (Fig. 3A).

When we introduced *Arabidopsis* PBAC1 or PBAC2 into the corresponding *doa5-1 Δpba1* and *doa5-1 Δpba2* backgrounds in various combinations, rescue of the canavanine hypersensitivity phenotype was not evident (Fig. 3A). Neither was PBAC5 effective, initially suggesting that the *Arabidopsis* chaperones are sufficiently distinct to prevent cross complementation, as was the case with UMP1 (Gemperline et al., 2019). However, when all three *Arabidopsis* chaperones were co-expressed in *doa5-1 Δpba1 Δpba2* cells,

Journal of Cell Science (2020) 133, jcs249862. doi:10.1242/jcs.249862

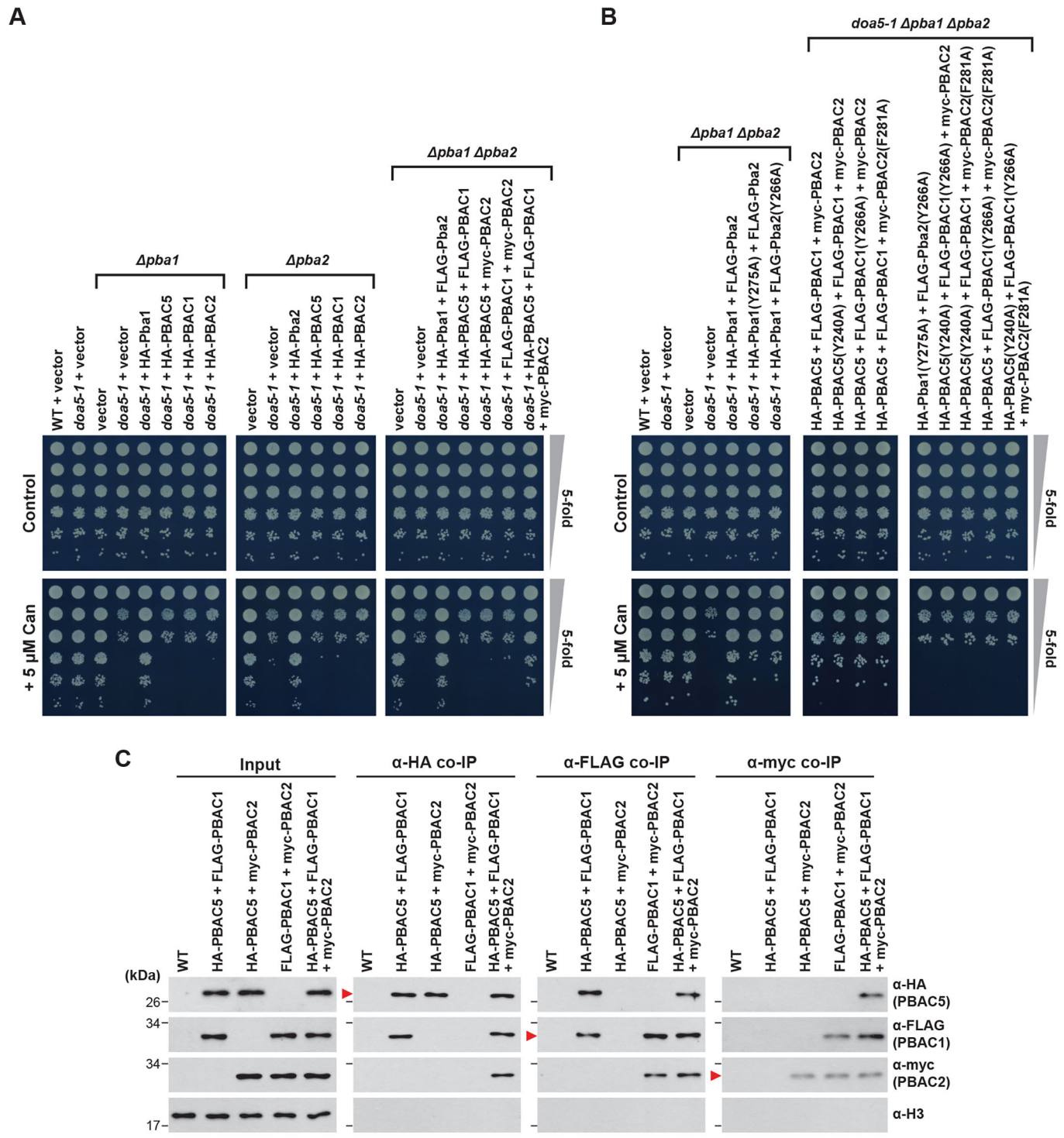

Fig. 3. The *Arabidopsis* PBAC5–PBAC1–PBAC2 complex rescues yeast mutants missing the Pba1 and Pba2 chaperones. (A,B) Yeast strains lacking Pba1 and/or Pba2 in the *doa5-1* background were applied in 5-fold serial dilutions onto medium with or without 5 µM canavanine (Can) and grown for 48 h at 30°C. (A) The Can hypersensitivity of the yeast *Δpba1*, *Δpba2* and *Δpba1 Δpba2* strains containing the *doa5-1* mutation are rescued by co-expression of PBAC1, PBAC2 and PBAC5. (B) Rescue of the Can hypersensitivity of the yeast *Δpba1 Δpba2* strain requires an intact HbYX/HbF motif in two of the three *Arabidopsis* chaperones. (C) PBAC1 tethers PBAC5 to PBAC2 in a hetero-trimeric complex. WT cells or *doa5-1 Δpba1 Δpba2* cells expressing the indicated *Arabidopsis* chaperones were immunoprecipitated with anti-HA, anti-FLAG or anti-myc antibody beads. Input and bound proteins were visualized by immunoblotting with the indicated antibodies. Immunodetection of histone H3 was included as a negative control. The red arrowheads identify the protein directly immunoprecipitated from each lysate.

canavanine hypersensitivity was nearly abolished (Fig. 3A). This partial rescue implied that a hetero-trimeric PBAC5–PBAC1–PBAC2 complex exists that can functionally replace the yeast Pba1–Pba2 heterodimer.

Considering that the HbYX motif in PBAC5 might be of similar importance as those predicted for PBAC1 and PBAC2, we next tested the need for these sequences in complementing *doa5-1*

Journal of Cell Science (2020) 133, jcs249862. doi:10.1242/jcs.249862

Δpba1 Δpba2 cells, using mutants in which the tyrosine (in PBAC1 and PBAC5) or phenylalanine (in PBAC2) residues were replaced with alanine. Whereas the wild-type (WT) versions of yeast Pba1 and Pba2 rescued the canavanine hypersensitive phenotype, mutations impacting either HbYX sequence blocked full complementation, again demonstrating that this motif in both Pba1 and Pba2 is required for full chaperone function in yeast (Fig. 3B; Kusmierczyk et al., 2011). However, when the three *Arabidopsis* chaperones were co-expressed, we unexpectedly found that the PBAC5–PBAC1–PBAC2 complex could still partially rescue the canavanine hypersensitivity of the *doa5-1 Δpba1 Δpba2* cells if only a single HbYX or HbF motif was altered, but not if two out of the three motifs were altered (Fig. 3B). Thus, in both yeast and *Arabidopsis*, at least two HbYX or HbF motifs in the Pba1–Pba2 and PBAC5–PBAC1–PBAC2 chaperone complexes are needed.

To support assembly of a hetero-trimeric PBAC5–PBAC1–PBAC2 complex with PBAC1 acting as the central tether, we exploited the complemented yeast strains described above to perform paired co-immunoprecipitation assays. As shown in Fig. 3C, the trimer could only be immunoprecipitated from cells expressing *FLAG–PBAC1* along with both *myc–PBAC2* and *HA–PBAC5*, and when the *FLAG–PBAC1* gene was omitted, no co-immunoprecipitation of myc–PBAC2 and HA–PBAC5 was observed. For further confirmation and to avoid potential complications provided by other yeast proteasome components or chaperones, *E. coli*-expressed *Arabidopsis* PBAC1, PBAC2 and PBAC5 bearing N-terminal glutathione *S*-transferase (GST), 6His and HA tags, respectively, were affinity purified via their corresponding tags (Fig. 2D) and mixed in various combinations for *in vitro* pulldown assays using anti-HA antibody or nickel-nitrilotriacetic acid (Ni-NTA) chelate beads. Again, only when GST–PBAC1 was present could we simultaneously enrich for both 6His–PBAC2 and HA–PBAC5 (Fig. 2E).

Arabidopsis mutants lacking PBAC5 show multiple proteasome-related defects

To support their roles in *Arabidopsis* CP assembly, we examined the functions of PBAC1, PBAC2 and PBAC5 genetically using a collection of T-DNA insertion mutants, whose T-DNA positions were confirmed by genomic DNA sequencing around the insertion sites (Fig. 4A; Fig. S1B). Analyses by reverse transcription (RT)-PCR failed to detect corresponding full-length mRNAs in several of the mutants when homozygous, including the sole *pbac1* allele (*pbac1-1*), the two *pbac2* alleles (*pbac2-1* and *pbac2-2*) and one *pbac5* allele (*pbac5-3*), suggesting that these lines represent strong, if not null, alleles (Fig. 4B,C). Two additional *pbac5* alleles (*pbac5-1* and *pbac5-2*) were identified that had reduced transcript abundance; reverse transcription quantitative PCR (RT-qPCR) assays revealed that both had ∼25% of the mRNA expression found in WT (Fig. 4B,C). Interestingly, mRNA levels for *PBAC5* were slightly elevated in the *pbac1* and *pbac2* null mutants compared to levels in WT (Fig. 4C), possibly indicating that the proteasome-stress regulon controlled by the NAM/ATAF1/CUC2-53 (NAC53) and NAC78 transcription factor pair was activated (Gladman et al., 2016), which would be consistent with a block in proteasome assembly (see below).

Under standard growth conditions, plants homozygous for each mutation appeared phenotypically normal and produced viable seeds, indicating that none of the three chaperones are essential to *Arabidopsis* by themselves. With a focus on PBAC5, we next tested whether the *pbac5-3* mutant seedlings were susceptible to proteotoxic stress, as were mutants in the CP maturation factor UMP1a (Gemperline et al., 2019). We first measured the growth response of the seedlings when exposed to various concentrations of MG132 or canavanine, using the response of double mutant seedlings lacking NAC53 and NAC78 as a positive control (Gladman et al., 2016). WT seedlings grew reasonably well on low doses of MG132 or canavanine beginning at germination (25 or 5 µM, respectively), but stalled at higher concentrations (50 µM MG132 or 25 µM canavanine), whereas growth of the *nac53-1 nac78-1* seedlings was strongly inhibited by even low drug doses (Fig. 4D,E). The *pbac5-3* seedlings also displayed a strong hypersensitivity to both treatments, though not to the same extent as *nac53-1 nac78-1* seedlings, indicating that this chaperone is important but not critical for proteostasis (Fig. 4D,E).

To confirm that this proteotoxic-stress phenotype was linked to the absence of PBAC5, we tested the sensitivity of homozygous *pbac5-3* seedlings complemented with a transgene expressing either WT HA–PBAC5 or an HA–PBAC5(ΔHbYX) variant in which the HbYX motif was deleted. For this purpose, transgenic lines were selected that expressed similar levels of the *HA–PBAC5* and *HA–PBAC5(ΔHbYX)* loci relative to WT *PBAC5*, as judged by RT-qPCR analysis (Fig. 4F), and that accumulated similar levels of the HA–PBAC5 and HA–PBAC5(ΔHbYX) proteins, as determined using immunoblot analysis of seedling extracts with anti-HA antibodies (Fig. 4G). The *HA–PBAC5* transgene successfully rescued the MG132 and canavanine hypersensitivity of *pbac5-3* seedlings, whereas the *HA–PBAC5(ΔHbYX)* transgene did not (Fig. 4D,E), thus firmly connecting the observed phenotypes to PBAC5, and demonstrating that the HbYX motif is essential for its activity *in planta*.

In addition to the proteotoxic stress hypersensitivity, *pbac5-3* seedlings displayed other proteasome-related defects. As measured with the fluorogenic succinyl-LLVY-AMC substrate (Kisselev and Goldberg, 2005), *pbac5-3* and *HA–PBAC5(ΔHbYX) pbac5-3* seedlings had ∼55% less CP activity as compared to WT or *HA–PBAC5 pbac5-3* seedlings, consistent with compromised CP assembly (Fig. 4H). The *pbac5-3* seedlings also activated the proteasome-stress regulon, as evidenced by the 1.5- to 2-fold increase in transcripts encoding an array of CP and RP subunits, as determined by RT-qPCR (Fig. S3B). Furthermore, *pbac5-3* seedlings hyper-accumulated ubiquitin conjugates, as predicted to occur if proteasome levels became insufficient (Fig. S3A). Notably, both activation of the proteasome-stress regulon and the increase in ubiquitin conjugates were suppressed by complementing the *pbac5-3* mutant with the *HA–PBAC5* transgene, but not with the *HA–PBAC5(ΔHbYX)* transgene (Fig. S3A,B). The *pbac5-1* and *pbac5-2* knockdown mutants also displayed similar aberrant phenotypes, but at levels intermediate between those of WT and the *pbac5-3* null mutant, consistent with attenuated but not abolished expression of *PBAC5* (Fig. 4C; Figs S4A–C, S5A).

Mutants lacking PBAC1 and PBAC2 show similar phenotypes to *pbac5-3*

Expecting that PBAC1 and PBAC2 work together with PBAC5 in CP assembly, we predicted that mutations eliminating PBAC1 or PBAC2 would similarly impact proteotoxic stress sensitivity, proteasome activity, proteasome-stress regulon activation and ubiquitin conjugate levels, as compared to the *pbac5-3* mutant. Besides testing the *pbac1-1*, *pbac2-1* and *pbac2-2* single null mutants (Fig. 5A), we also examined higher-order mutant combinations, including the homozygous *pbac1-1 pbac2-1 pbac5-3* triple mutant generated by introgression. Surprisingly, even the triple mutant was viable and grew indistinguishably to WT under standard conditions, again showing that none of the three chaperones are essential to

Journal of Cell Science (2020) 133, jcs249862. doi:10.1242/jcs.249862

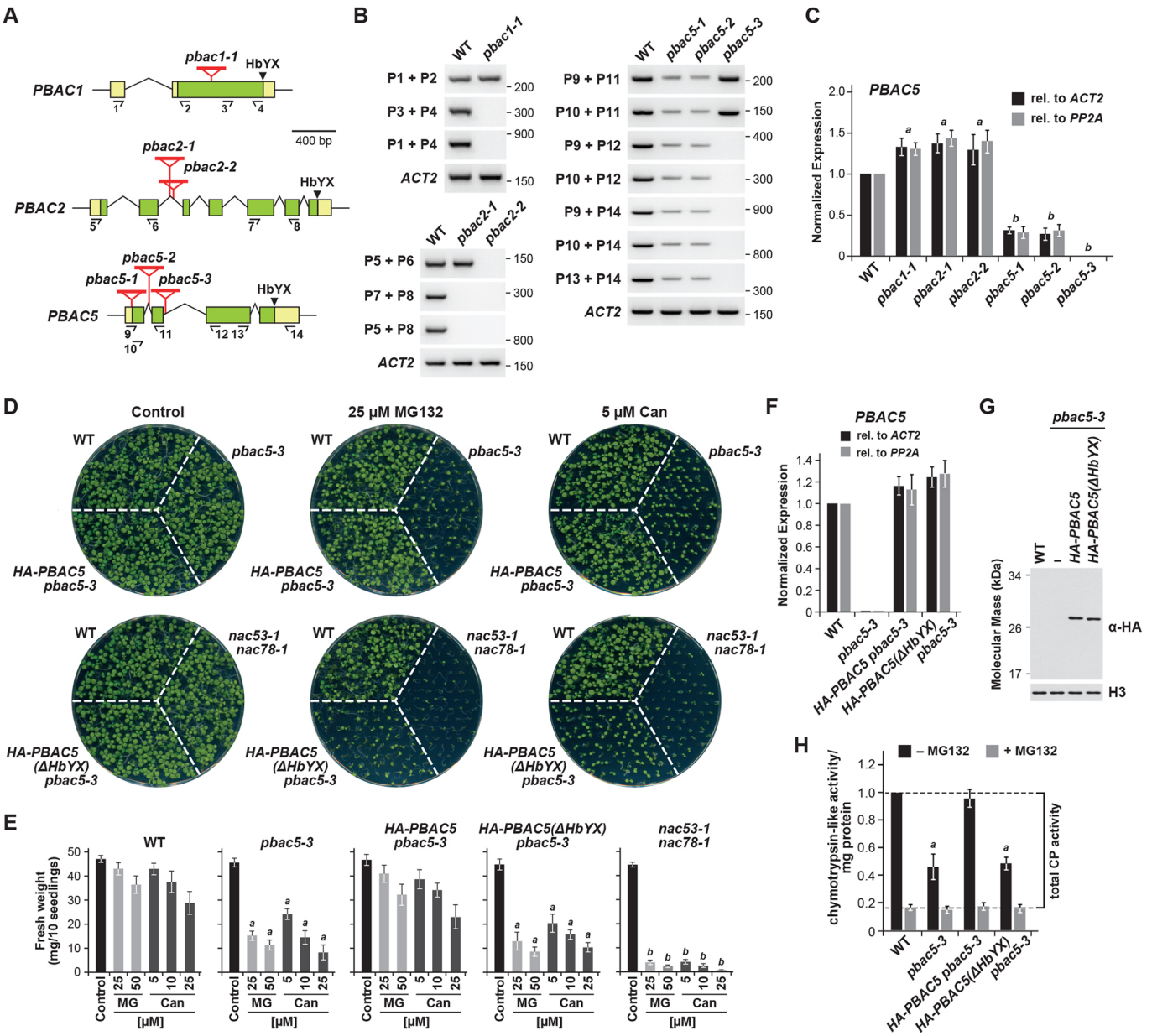

Fig. 4. *Arabidopsis pbac5* mutants have reduced 26S proteasome activity and are hypersensitive to proteotoxic stress. (A) Diagrams of the *Arabidopsis PBAC1*, *PBAC2* and *PBAC5* genes. The boxes represent coding regions (green) or UTRs (yellow), and lines represent introns. T-DNA insertions are indicated by the red triangles; insertion sites are shown in Fig. S1B. Half-arrows locate the oligonucleotide primers used for RT-PCR analysis in B. The black arrowheads indicate the HbYX/HbF motifs. (B) RT-PCR analysis of the *PBAC1*, *PBAC2* and *PBAC5* transcripts in the T-DNA mutants using the indicated oligonucleotide primer pairs. Amplification of *ACT2* was used to confirm analysis of near equal amounts of cDNA. Numbers on the right represent size markers in base pairs. (C) *PBAC5* mRNA levels in the mutant backgrounds. Relative transcript abundance was determined by RT-qPCR, using the *ACT2* and *PP2A* genes as internal reference standards. All data points were normalized to WT; bars represent mean±s.d. from three independent biological replicates, each with three technical replicates. (D) Seedlings of the indicated genotypes were grown on medium containing either DMSO (control), 25 µM MG132 or 5 µM canavanine (Can). The *nac53-1 nac78-1* double mutant was used as a positive control. (E) Quantification of seedling sensitivity to MG132 or Can. Shown is the mean±s.d. fresh weight from three biological replicates of 10 seedlings grown as in D. (F) *PBAC5* mRNA levels in WT, *pbac5-3*, or complemented *pbac5-3* seedlings. Relative transcript abundance was determined as in C. (G) Detection of the HA–PBAC5 and HA–PBAC5(ΔHbYX) proteins in the complemented lines. Total protein extracts were immunoblotted with anti-HA antibodies. Immunodetection of histone H3 was used to confirm near equal protein loading. (H) CP peptidase activity is reduced in the *pbac5-3* mutant. CP activity was measured in the presence or absence of 80 µM MG132 using the succinyl-LLVY-AMC substrate. Data were normalized to WT; bars represent the mean±s.d. of three biological replicates, each with three technical replicates. The letters in C, E and H indicate values that are significantly different from one another and the control, as determined by one-way ANOVA followed by Tukey's post hoc test (P<0.05).

Arabidopsis. However, analysis of the entire mutant collection with respect to proteasome function revealed a similar severity for a number of responses, suggesting that the three proteins work collectively in proteasome assembly. As examples, the *pbac1-1* and *pbac2-1* single homozygous mutants, either alone or in combination with *pbac5-3* as double or triple mutants, displayed a similar hypersensitivity to MG132 and canavanine as the *pbac5-3* mutant alone (Fig. 5A,B). These single, double and triple mutant combinations also had equal activation of the proteasome-stress regulon, as judged by increased levels of mRNAs encoding CP and

Journal of Cell Science (2020) 133, jcs249862. doi:10.1242/jcs.249862

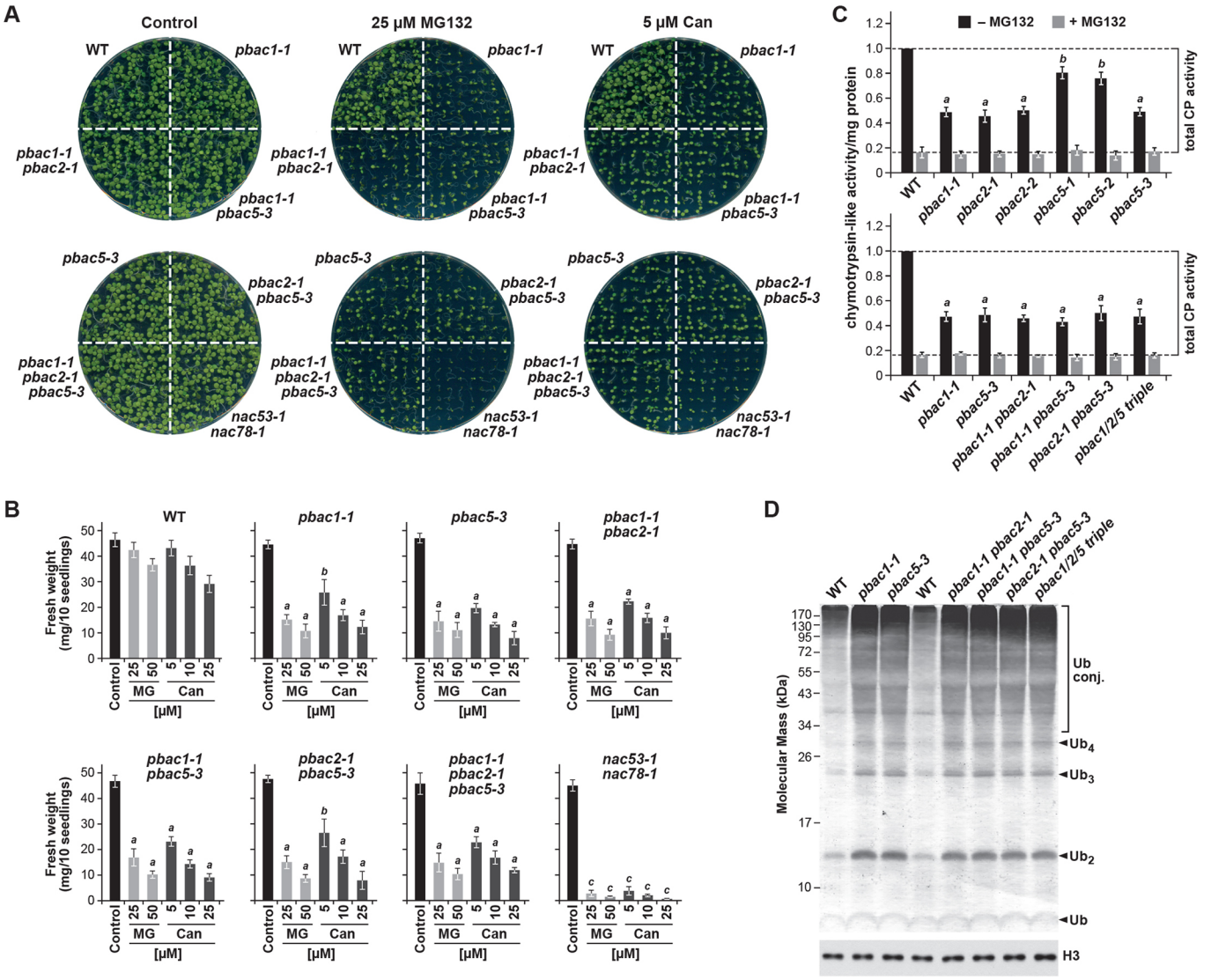

Fig. 5. *Arabidopsis* mutants missing PBAC1, PBAC2 and/or PBAC5 have reduced 26S proteasome activity, are hypersensitive to proteotoxic stress and hyper-accumulate ubiquitin conjugates. (A) Homozygous *pbac1-1*, *pbac2-1* and *pbac5-3* seedlings are hypersensitive to proteotoxic stress. Seedlings were grown as in Fig. 4D in the presence of either DMSO (control), MG132 or canavanine (Can). (B) Quantification of seedling sensitivity to MG132 or Can. Shown is the mean±s.d. fresh weight from three biological replicates of 10 seedlings grown as in A. (C) CP peptidase activity was reduced in the *pbac1*, *pbac2* and *pbac5* single, double and triple mutants. CP activity was measured as in Fig. 4H. Data were normalized to WT; bars represent the mean±s.d. of three biological replicates, each with three technical replicates. (D) The *pbac1-1*, *pbac2-1* and *pbac5-3* seedlings hyper-accumulate ubiquitin conjugates. Total protein extracts were immunoblotted with anti-ubiquitin antibodies. Ubiquitin conjugates and polyubiquitin chains of the indicated lengths are indicated by the bracket and arrowheads, respectively. The letters in B and C indicate values that are significantly different from one another and the control, as determined by one-way ANOVA followed by Tukey's post hoc test (P<0.05).

RP subunits of the 26S proteasome (Fig. S5A,B), and a similar hyper-accumulation of ubiquitin conjugates (Fig. 5D). All the mutants also had near equal reductions in proteasome activity, based on the succinyl-LLVY-AMC substrate (Fig. 5C).

We previously showed that *Arabidopsis* mutants with attenuated expression of the CP maturation factor UMP1 are hypersensitive to salt and drought stress (Gemperline et al., 2019). Here, we tested whether our panel of *pbac1*, *pbac2* and *pbac5* mutants were similarly compromised, using the *pbe1-2* mutant affecting the CP subunit PBE1 (β_5) as a positive control (Han et al., 2019). Growth of the single and double mutants, and the *pbac1-1 pbac2-1 pbac5-3* triple mutant, was strongly dampened in the presence of NaCl, mannitol or the drought-responsive hormone abscisic acid (ABA) when used at concentrations that only mildly suppressed growth of WT *Arabidopsis*, although the effect was less pronounced than for *pbe1-2* seedlings (Fig. S6A–D). For the *pbac5-3* line, these sensitivities were rescued by the *HA–PBAC5* transgene but not by *HA–PBAC5(ΔHbYX)*, again confirming the importance of the HbYX sequence to PBAC5 activity (Fig. S7A,B).

The PBAC5–PBAC1–PBAC2 complex is required for efficient proteasome assembly

To definitively assess the importance of the PBAC5–PBAC1–PBAC2 trimer to 26S proteasome assembly, we monitored protease integrity using glycerol gradient fractionation. Here, total seedling extracts from WT, the single *pbac1-1*, *pbac2-1* and *pbac5-3* mutants, the triple mutant, and the *pbac5-3* mutant complemented with the *HA–PBAC5* or *HA–PBAC5(ΔHbYX)* transgenes were analyzed, with the inclusion of ATP at all steps to stabilize the holo-proteasome. Consistent with previous results (Book et al., 2010;

Journal of Cell Science (2020) 133, jcs249862. doi:10.1242/jcs.249862

Gemperline et al., 2019; Lee et al., 2011), a single 26S species containing both the CP and RP was detected in WT samples by immunoblotting the fractions with a panel of proteasome subunit antibodies (Fig. 6). By contrast, samples from *pbac1-1*, *pbac2-1* and *pbac5-3* single mutant seedlings, and the *pbac1-1 pbac2-1 pbac5-3* triple mutant, amassed not only the 26S species but also an RP particle of intermediate sedimentation and substantial amounts of CP α- and β-subunits at the top of the gradient, but little to no free CP (Fig. 6; Fig. S4D), all consistent with CP assembly defects (Gemperline et al., 2019; Hirano et al., 2005; Lee et al., 2011).

The sedimentation positions of the CP subunits likely reflected the accumulation of free proteins or partially assembled CP α-rings with or without β-subunits, as was previously seen for mutants missing UMP1 (Gemperline et al., 2019), whereas the positions of the RP subunits were consistent with fully assembled free RP (Gemperline et al., 2019; Lee et al., 2011). Notably, the assembly defects were no worse in the *pbac1-1 pbac2-1 pbac5-3* triple mutant as compared to the individual single mutants, again supporting the notion that the three chaperones work together (Fig. 6). These assembly defects were absent in *pbac5-3* plants expressing WT HA–PBAC5, but remained in plants expressing HA–PBAC5(ΔHbYX), again indicating that the HbYX motif in PBAC5 is critical for efficient CP assembly (Fig. 6). Interestingly, the HA–PBAC5 protein was found in the top four fractions of the gradient, consistent with an association with CP assembly intermediates, which we assume are in low abundance relative to the fully assembled CP. In contrast, the HA–PBAC5(ΔHbYX) protein was almost exclusively in the top fraction, suggesting that it was free protein precluded from associating with α-subunits without its HbYX motif (Fig. 6).

We note that RPN5, but not the other *Arabidopsis* RPN subunits tested, also consistently sedimented with a distinct species, which was slightly smaller than free RP (Fig. 6). The nature of this particle is unknown but could reflect RPN5 also integrating into the structurally related COP9 signalosome complex, as seen in yeast (Yu et al., 2011).

PBAC5 likely binds between the α_4 and α_5 subunits of the CP

To better understand how PBAC5 interacts with proteasomes, we identified, using MS, the collection of *Arabidopsis* proteins that bind HA–PBAC5. MS analysis of the anti-HA antibody eluants prepared from *HA–PBAC5 pbac5-3* seedlings in the absence of MG132 not only detected PBAC5 but also several CP α-subunits and other CP assembly chaperones that were enriched as compared to their levels in eluants from WT seedlings (Fig. 7). The most significantly enriched were the α-subunits PAD1 (α_4), PAE1 and PAE2 (both α_5), and the chaperones PBAC1 and UMP1b. The enrichment of PBAC1 was consistent with our demonstrations that PBAC1 and PBAC5 interact (Figs 2B,C,E and 3C), whereas those for PAD1, PAE1 and PAE2 were consistent with PBAC5 specifically binding to and aiding in the association of these two α-subunits, which are adjacent in the mature CP.

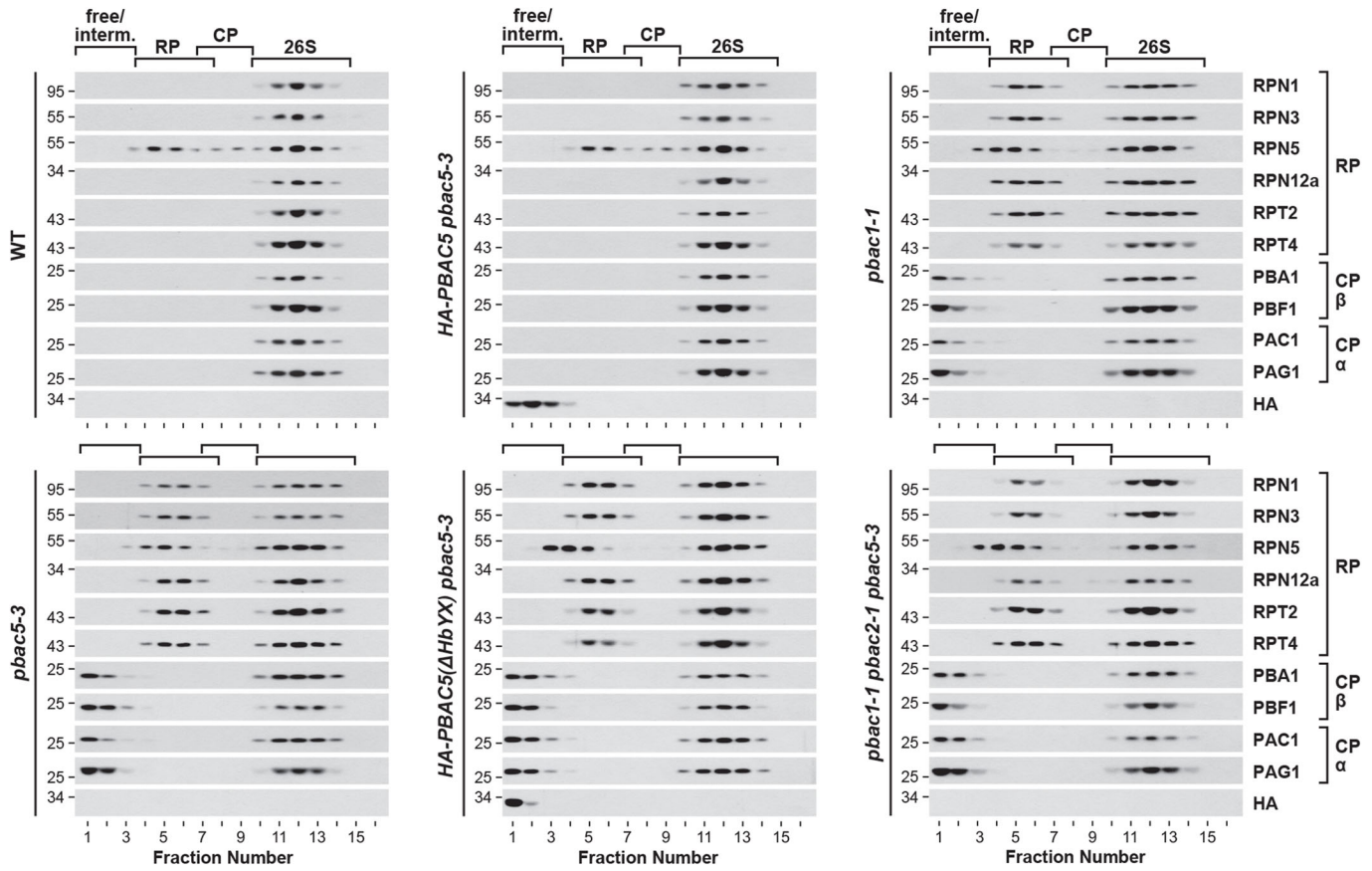

Fig. 6. *Arabidopsis* mutants missing PBAC1, PBAC2 and/or PBAC5 accumulate 26S proteasome assembly intermediates. Total protein extracts from WT, *pbac1-1*, *pbac5-3*, *pbac1-1 pbac2-1 pbac5-3*, or *pbac5-3* seedlings complemented with the *HA–PBAC5* or *HA–PBAC5(ΔHbYX)* transgenes were subjected to glycerol gradient fractionation and analyzed by immunoblotting with antibodies against the indicated proteasome subunits. The predicted positions of free proteasome subunits (free), assembly intermediates (interm.), CP, RP and the holo-26S proteasome are indicated by the horizontal brackets. Numbers on the left represent molecular mass markers in kDa. Analysis of the *pbac2-1* mutant is in Fig. S4D.

Journal of Cell Science (2020) 133, jcs249862. doi:10.1242/jcs.249862

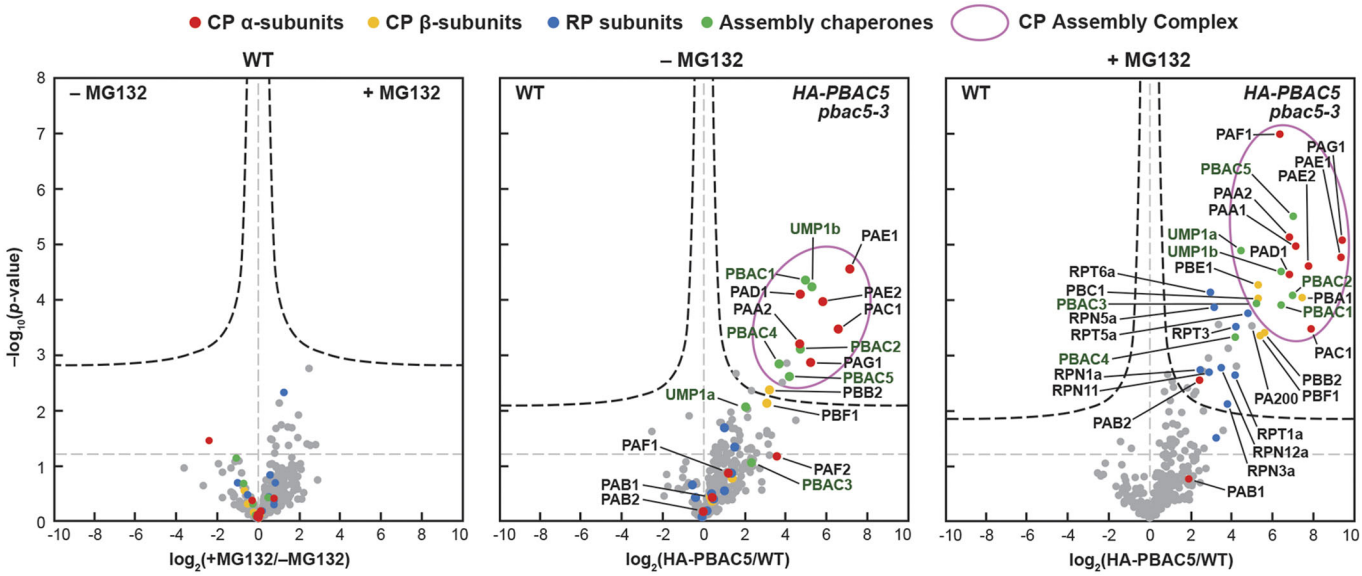

Fig. 7. *Arabidopsis* PBAC5 interacts with a CP α-ring subcomplex containing PBAC1, PBAC2 and UMP1. Protein extracts from WT or *HA–PBAC5 pbac5-3* seedlings treated with DMSO (–MG132) or 50 µM MG132 were immunoprecipitated with anti-HA agarose beads, trypsinized, and subjected to MS. Volcano plots of the detected proteins comparing the $\log_2$ fold difference in abundance and $-\log_{10}$ *P*-value of significance. Relevant 26S proteasome subunits and chaperones are labeled. CP α-subunits, CP β-subunits, RP subunits and assembly chaperones are indicated by red, yellow, blue and green dots, respectively. A possible CP assembly complex is highlighted by the ovals. The dashed horizontal and vertical gray lines identify no change in abundance and a *P*-value of 0.05, respectively. The dashed black lines demarcate proteins that were differentially represented in the one sample relative to the other, as judged by a significance analysis of microarray (SAM) test using a FDR of 0.01.

Also moderately enriched were the α-subunits PAA2 (α_1), PAC1 (α_3) and PAG1 (α_7), plus the PBAC2 and PBAC4 chaperones (Fig. 7), suggesting that these five CP α-subunits, four assembly chaperones and UMP1 represent an early CP α-ring assembly module (Fig. 7). Two isoforms of α_2 (PBA1 and PBA2) and α_6 (PAF1 and PAF2), and the PBAC3 and UMP1a chaperones, were also identified, but only at amounts well below the level of significance, and with little enrichment compared to their levels in the eluants from WT (Fig. 7). We also note that, besides PBB2 (β_2) and PBF1 (β_6), no other β-subunits were detected, nor was the PA200 regulator evident, again consistent with these HA–PBAC5 enriched species reflecting early assembly intermediates consisting of just α-subunits and their assembly chaperones and other factors.

Treating *Arabidopsis* with MG132 leads to an acceleration of 26S proteasome synthesis, mainly through an activation of the proteasome-stress regulon that controls expression of most, if not all, RP and CP subunits, and associated assembly chaperones and maturation factors (Gemperline et al., 2019; Gladman et al., 2016). MS analysis of MG132-treated WT or *HA–PBAC5 pbac5-3* detected a significantly increased number of these factors, now including all five PBAC chaperones, UMP1a, UMP1b, and even PA200 (Fig. 7). Isoforms for all seven α-subunits and six of the seven β-subunits [the exception being PBG1 (β_7)] were also evident, along with a collection of RP subunits with lower significance (Fig. 7). Because β_7 is the last subunit to be integrated into the complex prior to formation of CP half-barrels, its absence is consistent with the immunoprecipitations being enriched in 15S intermediates. Taken together, the MS analysis supported the association of PBAC5 with an α-ring intermediate also containing PBAC1, with the enrichment of PAD1 (α_4), PAE1 and PAE2 (both α_5) confirming direct binding to this α-ring pair.

PBAC5 proteins are not widely conserved throughout evolution

Although PBAC5 was clearly found to be present throughout the plant kingdom (Fig. 1A), no obvious homologs were detected in humans or yeast, leading to the notion that PBAC5 is a plant-specific chaperone. To help support this possibility, we performed profile HMM searches of the GenBank DNA sequence database (https://www.ncbi.nlm.nih.gov/genbank/), which identified 181 possible PBAC5 orthologs (Table S1). As predicted, a majority were plant sequences, with all taxa appearing to possess a PBAC5 homolog distinct from PBAC1 and PBAC2, including monocots, eudicots, gymnosperms and seedless plants, plus several green and brown algal species (*Chlamydomonas* spp., *Ectocarpus* spp., *Gonium* spp., *Micromonas* spp., and *Volvox* spp.; Fig. 8A). Surprisingly, 41 of the sequences were from non-plant genomes. Although many of these matches were of borderline significance initially, they became significant after creating specific HMM searches using the plant family to facilitate HMM-to-HMM comparisons.

Non-plant species with potential PBAC5 orthologs included a number of oomycetes (e.g. *Hyaloperonospora* spp., *Phytophthora* spp., *Pythium* spp., *Saprolegnia* spp., *Thraustotheca* spp.), and a few fungi and metazoans, although the distributions were sporadic. For example, all fungal sequences containing PBAC5 were from basal lineages (e.g. Chytridomycota, Mucoromycota, Neocallimastigomycota and Zoopagomycota) but, even within these lineages, only very few species encoded a likely ortholog (Fig. 8A; Table S1). The single celled protist *Sphaeroforma arctica* possesses a PBAC5-type sequence, but was the only holozoan representative. Remarkably, the few metazoan PBAC5 sequences identified were from disparate organisms that included the fish-like lancelet *Branchiostoma floridae*, the Japanese sea scallop *Mizuhopecten yessoensis*, the slime sponge *Oscarella carmela*, the sea snail *Pomacea canaliculata*, brachiopods of the *Lingula* genus and flatworms of the *Macrostomum* genus (Fig. 8A; Fig. S8).

Subsequent searches using the entire PBAC5 family also revealed significant matches to the families encompassing the archaeal and bacterial Pba chaperones that assemble the homo-heptameric CP α-ring (Kusmierczyk et al., 2011), thus helping establish that PBAC5 is a member of the Pba/PAC/PBAC superfamily. Because

Journal of Cell Science (2020) 133, jcs249862. doi:10.1242/jcs.249862

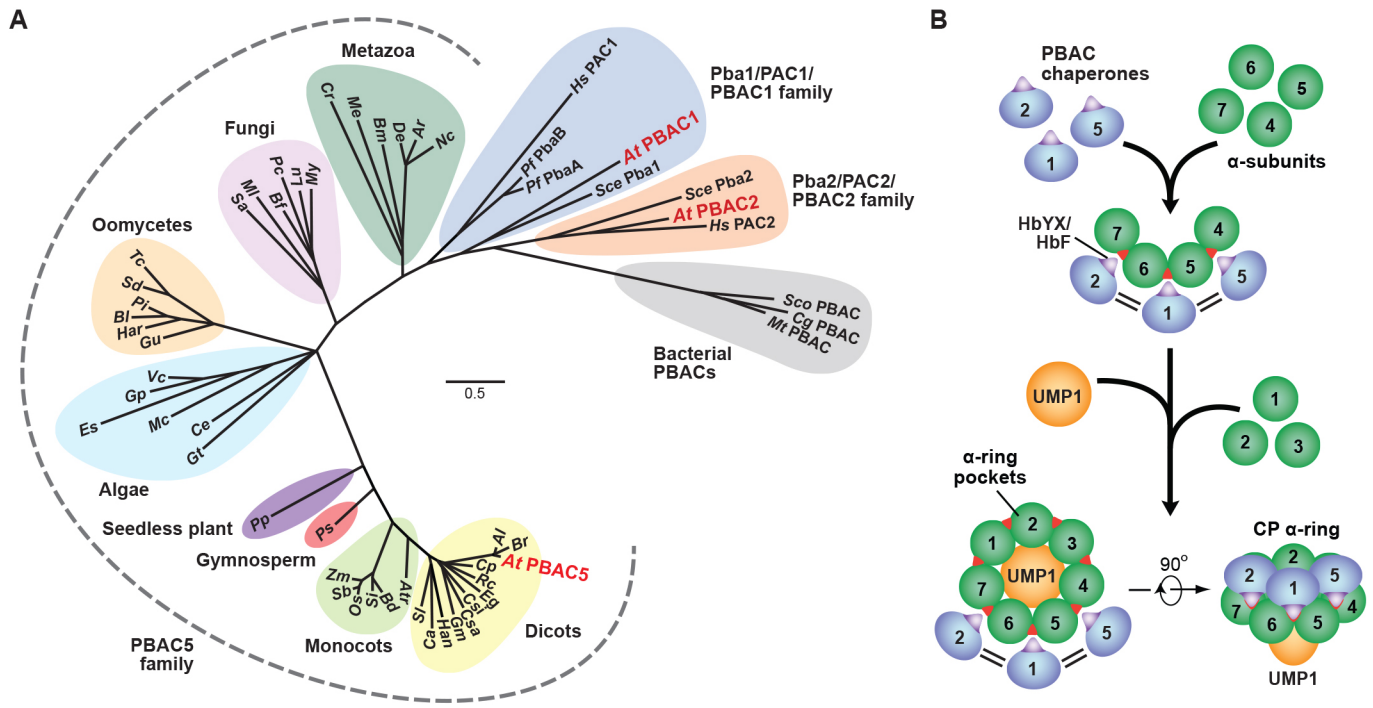

Fig. 8. Possible PBAC5 orthologs in various fungal, metazoan and oomycete species, and a model for PBAC5-mediated CP α-ring assembly. (A) Phylogenetic analysis of the expanded PBAC5 family (dashed line), and its relationship to the eukaryotic Pba1/PAC1/PBAC1 and Pba2/PAC2/PBAC2 families, and the bacterial PBAC family. Representative members from plants, fungi, metazoans and oomycetes were subjected to phylogenetic analysis using the neighbor-joining method, and the resulting consensus tree was displayed using FigTree. The scale bar represents substitutions per site. An alignment of representative sequences is in Fig. S8. Species abbreviations are in the Materials and Methods. (B) A model for CP α-ring assembly. The PBAC5, PBAC1 and PBAC2 chaperones (blue) associate as a trimer to assemble an ordered α-ring complex containing α_4–α_7 (green) through interactions between the HbYX/HbF motifs in the chaperones and hydrophobic pockets at the α_4–α_5, α_5–α_6, and α_6–α_7 interfaces, respectively. UMP1 docks to the α_4–α_7 subcomplex to help integrate α_1–α_3 into the heptameric α-ring, likely in association with PBAC3–PBAC4 (not shown). The HbYX/HbF motifs and α-subunit pockets are indicated by the purple and red triangles, respectively.

all of the PBAC5-containing species also possessed conventional PBAC1 and PBAC2 members, a likely scenario is that PBAC5 split from the Pba1–Pba2/PAC1–PAC2 branches early in evolution, and was later lost in most lineages, possibly accompanied by a gain of function for the Pba1–Pba2/PAC–PAC2 dimer that resulted in PBAC5 becoming dispensable.

DISCUSSION

26S proteasomes are large proteolytic machines with a sophisticated architecture built from multiple heteromeric rings (Bhattacharyya et al., 2014; Greene et al., 2020; Marshall and Vierstra, 2019), which in eukaryotes must be assembled in correct register from evolutionarily related subunits (Gille et al., 2003). It is therefore unsurprising that proteasome assembly is a complicated, multistep process driven by the sequential action of various extrinsic assembly chaperones and maturation factors (Howell et al., 2017; Marshall and Vierstra, 2019; Rousseau and Bertolotti, 2018). The initial step in CP assembly is particularly challenging, requiring formation of a hetero-heptameric ring of related α-subunits, which is promoted by two hetero-dimeric chaperones (Pba1–Pba2 and Pba3–Pba4 in yeast) that help ensure correct subunit positioning and stoichiometry (Hirano et al., 2005, 2006; Kock et al., 2015; Kusmierczyk et al., 2008, 2011; Le Tallec et al., 2007; Stadtmueller et al., 2012; Wani et al., 2015; Wu et al., 2018; Yashiroda et al., 2008). Additionally, at least in yeast, α_1 subunit integration is rate limiting during assembly (Howell et al., 2019), hence chaperones are required to prevent premature association of incomplete proteasome intermediates. Upon α-ring formation, the Ump1 maturation factor then aids consecutive docking of the β-subunits onto the α-ring template (Burri et al., 2000; Li et al., 2007; Ramos et al., 1998).

Despite extensive knowledge obtained from yeast and mammalian studies, the low sequence identities of assembly chaperones across kingdoms have challenged understanding of proteasome assembly in plants (Gemperline et al., 2019; Wang et al., 2019). Recently, we overcame this hurdle through the MS analysis of *Arabidopsis* proteasomes, which discovered a suite of CP- and RP-specific interacting proteins, several of which are confirmed homologs of the yeast and mammalian Pba/PAC CP α-ring assembly chaperones and UMP1, despite low sequence homology (Gemperline et al., 2019). Here, we demonstrate that the CP-interacting protein PBAC5 is an additional assembly chaperone in *Arabidopsis* that, like its relatives PBAC1 and PBAC2, contains the signature C-terminal HbYX motif that promotes CP binding. Through various interaction studies, we showed that PBAC5 assembles into an ordered PBAC5–PBAC1–PBAC2 chaperone hetero-trimer, which then binds to a subcomplex of the CP, comprising almost exclusively the α-ring subunits α_4, α_5, α_6, α_7 and possibly α_3, which might represent the initial step in plant α-ring assembly.

As predicted, *Arabidopsis pbac5* mutants displayed numerous phenotypes consistent with CP construction defects. Included were: (1) the accumulation of CP assembly intermediates apparently stalled in α-subunit integration; (2) reduced levels of enzymatically active proteasomes; (3) a hypersensitivity to proteotoxic stress induced by proteasome inhibition or the amino acid analog canavanine; (4) a hyper-accumulation of ubiquitin conjugates, presumably caused by proteasome insufficiency; and (5) an activation of the proteasome-

stress regulon that attempts to overcome this insufficiency by promoting new proteasome synthesis. Also observed were hypersensitivities of *Arabidopsis* seedlings to salt and osmotic stress, as was the case for mutants missing the UMP1a chaperone or carrying the *pbe1-2* allele compromising the β_5 subunit PBE1 (Gemperline et al., 2019; Han et al., 2019). In all cases, these aberrant *pbac5* phenotypes could be rescued by re-introducing WT HA–PBAC5, but not by a version of PBAC5 lacking the HbYX motif, thus confirming the importance of this sequence to PBAC5 activity. Subsequent genetic analysis of the *pbac1*, *pbac2* and *pbac5* mutants, alone or in combination, revealed that all three chaperones collectively promote α-ring assembly, with their absence generating the same phenotypic severities described above.

Notably, although the *Arabidopsis* PBAC1 and PBAC2 proteins together failed to rescue a yeast mutant lacking the Pba1–Pba2 dimer, the PBAC5–PBAC1–PBAC2 trimer was mostly successful, implying that the contacts provided by *Arabidopsis* PBAC1 and PBAC2 are alone insufficient for yeast α-ring assembly, and that PBAC5 provides additional contact(s) to overcome this apparent weak affinity. However, this stronger binding does not appear to depend on the HbYX motif in PBAC5, because the PBAC1, PBAC2 and PBAC5(Y240A) combination, in which the central tyrosine in the HbYX motif of PBAC5 was replaced with an alanine, was equally successful as the WT version. Our observations that the HbYX contact in PBAC5 was essential to its activity in *Arabidopsis*, but not in yeast, argues that additional interactions beyond the HbYX motif participate in α-subunit docking (Stadtmueller et al., 2012).

Our co-immunoprecipitation studies showing that HA–PBAC5 most strongly enriched for the PAD1 (α_4), PAE1 and PAE2 (α_5) subunits, together with the available crystal structure of yeast Pba1–Pba2 associated with the α-ring (Stadtmueller et al., 2012; Yashiroda et al., 2008), allowed us to develop a model for *Arabidopsis* CP α-ring assembly using the PBAC5–PBAC1–PBAC2 trimer (Fig. 8B). As in yeast and mammalian cells (Kusmierczyk et al., 2011; Stadtmueller et al., 2012), *Arabidopsis* PBAC1 would contact the shallow pocket at the α_5–α_6 interface through its HbYX motif, while PBAC2 would contact the α_6–α_7 interface through its HbF motif. PBAC5, through its binding to PBAC1, would then be placed directly over a potential pocket at the α_4–α_5 interface, thus helping PBAC5 encourage integration of α_4 alongside α_5 through binding by its HbYX motif and other surfaces. The entire trimer would then correctly register an α-ring tetramer consisting of α_4–α_5–α_6–α_7 (Wu et al., 2018). The dimeric PBAC3–PBAC4 chaperone, either alone or in combination with UMP1, could then help recruit α_2 and α_3, and ultimately α_1 to complete the heptameric α-ring.

Surprisingly, *Arabidopsis* mutants missing PBAC1, PBAC2 and PBAC5 were viable under standard growth conditions and still generated a pool of assembled 26S complexes, as opposed to the strong *ump1* mutations that are gametophytic lethal (Gemperline et al., 2019). One possibility is that the α-rings can self-associate, possibly with the help of only UMP1, PBAC3 and PBAC4. Alternative assembly routes, such as the complex comprising the α_1–α_4 and β_2–β_4 subunits seen in yeast, which can integrate the remaining subunits into half-proteasomes (Hammack et al., 2020; Panfair et al., 2015), might also exist. The diminished levels of the complete 26S particle seen in the chaperone mutants are clearly sufficient to maintain a healthy *Arabidopsis* proteome under normal growth conditions, but presumably become insufficient under conditions that induce proteotoxic stress, such as proteasome inhibitors, amino acid analogs and osmotic stress. Given that autophagy components are also upregulated upon proteasome stress (Gladman et al., 2016), it is likely that this recycling route is activated to augment proteolytic capacity under these conditions.

Our observations that PBAC5 has been retained in all plant and many oomycete species, but is absent from all but a few fungal and metazoan species, were both remarkable and puzzling. Because all species with PBAC5 orthologs also possess the conventional PBAC1 and PBAC2 chaperones, a possible scenario is that PBAC5 split from the PBAC1/PBAC2 branch early during evolution, and was later lost in most lineages (Albalat and Cañestro, 2016; Guijarro-Clarke et al., 2020). Given that PBAC5 is required for efficient plant proteasome assembly, and that all three subunits of the plant PBAC5–PBAC1–PBAC2 hetero-trimeric complex are needed to replace the Pba1–Pba2 chaperone in yeast, it might be the case that loss of PBAC5 conferred a selective advantage in most species, or that its loss was preceded by a gain of function for the Pba1–Pba2/PAC1–PAC2 dimer that rendered PBAC5 dispensable. Alternatively, we speculate that PBAC5 might be necessary to promote CP assembly in organisms more exposed to challenging environments. Because plants can tolerate remarkable extremes in temperature and other stresses (Dudler, 2013; Üstün et al., 2018), retaining PBAC5 along with PBAC1 and PBAC2 might aid CP assembly during adversity.

In summary, we describe here a novel proteasome CP α-ring assembly chaperone in *Arabidopsis* that is highly conserved in all plant and many oomycete species, but is absent in most fungi and metazoans. This discovery will aid future biochemical and genetic analyses of proteasome assembly in plants, which given its critical role in stress protection (Xu and Xue, 2019), might provide strategies to mitigate proteotoxic stress in agronomically important species. Given the weak homology seen between the PBAC5 family and those of PBAC1 and PBAC2, it is also intriguing to consider that other proteasome chaperones exist that are sufficiently divergent in sequence, or present at sufficiently low levels, to have thus far evaded detection.

MATERIALS AND METHODS

Sequence alignment, phylogenetic and expression analyses

The predicted full-length nucleotide and protein sequences of *Arabidopsis thaliana* PBAC1, PBAC2 and PBAC5 [obtained from the *Arabidopsis* Information Resource database version 10.1 (www.arabidopsis.org/)] were used as queries in PSI-BLAST searches for orthologous loci in other plant genomes available in the Joint Genome Initiative's Phytozome database (www.phytozome.net). Progressive alignments of the predicted full-length amino acid sequences were performed using Clustal Omega (www.clustal.org/omega/) with the default settings. Following minor manual editing, the final alignments were displayed using BoxShade version 3.2.3 (https://embnet.vital-it.ch/software/BOX_form.html). Bayesian phylogenetic analyses were then performed with MrBayes version 3.2.2 (Ronquist and Huelsenbeck, 2003) using the General Time Reversible evolutionary model with the mixed amino acid model and γ-distributed rate variation with a proportion of invariable sites, as previously described (Gemperline et al., 2019). The resulting consensus trees were displayed using FigTree version 1.4.2 (http://tree.bio.ed.ac.uk/software/figtree/).

Alternatively, to search for PBAC5 sequences in non-plant species, profile-HMM searches in sequence databases were performed using the generalized profiles method (Bucher et al., 1996) by iterative refinement, using a *P*-value <0.001 as an inclusion criterion for the next iteration cycle. Comparisons between different sequence families were performed using HHSEARCH (Söding, 2005) to generate HMM-to-HMM comparisons. Multiple sequence alignments were then created using the L-INS-I algorithm in the MAFFT package (Katoh et al., 2002), and phylogenetic trees were generated by the neighbor-joining method (Saitou and Nei, 1987) and displayed as above. Species abbreviations used are: *Al*, *Arabidopsis lyrata*; *Ath*, *Arabidopsis thaliana*; *Atr*, *Amborella trichopoda*; *Ar*, *Anaeromyces robustus*; *Bd*,

Brachypodium distachyon; *Bf*, *Branchiostoma floridae*; *Bl*, *Bremia lactucae*; *Bm*, *Basidiobolus meristosporus*; *Br*, *Brassica rapa*; *Ca*, *Capsicum annuum*; *Ce*, *Chlamydomonas eustigma*; *Cg*, *Corynebacterium glutamicum*; *Cp*, *Carica papaya*; *Cr*, *Coemansia reversa*; *Csa*, *Cucumis sativa*; *Csi*, *Citrus sinensis*; *De*, *Diversispora epigaea*; *Eg*, *Eucalyptus grandis*; *Es*, *Ectocarpus siliculosus*; *Gm*, *Glycine max*; *Gp*, *Gonium pectorale*; *Gt*, *Guillardia theta*; *Gu*, *Globisporangium ultimum*; *Han*, *Helianthus annuus*; *Har*, *Hyaloperonospora arabidopsidis*; *Hs*, *Homo sapiens*; *Lu*, *Lingula unguis*; *Mc*, *Micromonas commoda*; *Me*, *Mortierella elongata*; *Ml*, *Macrostomum lignano*; *Mt*, *Mycobacterium tuberculosis*; *My*, *Mizuhopecten yessoensis*; *Nc*, *Neocallimastix californiae*; *Os*, *Oryza sativa*; *Pc*, *Pomacea canaliculata*; *Pf*, *Pyrococcus furiosus*; *Pi*, *Phytophthora infestans*; *Ps*, *Picia sitchensis*; *Pp*, *Physcomitrella patens*; *Rc*, *Ricinus communis*; *Sa*, *Sphaeroforma arctica*; *Sb*, *Sorghum bicolor*; *Sce*, *Saccharomyces cerevisiae*; *Sco*, *Streptomyces coelicolori*; *Sd*, *Saprolegnia diclina*; *Si*, *Setaria italica*; *Sl*, *Solanum lycopersicum*; *Tc*, *Thraustotheca clavata*; *Vc*, *Volvox carteri*; *Zm*, *Zea mays*.

Raw transcript abundance data for the *Arabidopsis PBAC* family were downloaded from the Transcriptome Variation Analysis database (www.travadb.org/; Klepikova et al., 2016) and plotted in R (www.r-project.org/) using the heatmap.2 function, with centroided hierarchical clustering based on Pearson's correlation used as the distance function. All read counts were normalized to values ranging from 0 to 1 by the 'median-of-ratios' method, as in DESeq2 (Love et al., 2014), and then divided by the maximum expression for each gene.

Plant materials and growth conditions

All *A. thaliana* lines were derived from the Columbia-0 (Col-0) ecotype, except *pbac2-1* and *pbac2-2*, which were derived from the Col-3 ecotype. Details of all T-DNA insertion mutants and stable transgenic lines are provided in Tables S2 and S3. All insertion mutants were confirmed by genomic PCR using 5′ and 3′ gene-specific primers (LP and RP, respectively) in conjunction with an appropriate T-DNA left border-specific primer. Details of all oligonucleotide primers are provided in Table S4. The exact positions of the T-DNA insertions were determined by direct DNA sequencing of appropriate PCR products. Before analysis, all mutants were backcrossed at least three times to the WT Col-0 parent and then selfed to obtain homozygous progeny, using growth on medium containing 50 µg/ml kanamycin, 10 µg/ml BASTA and/or 6 µg/ml sulfadiazine for selection, depending on the source of the mutant.

Sterilized seeds (obtained via vapor-phase or liquid-phase sterilization) were vernalized at 4°C for 3–4 days and typically germinated on solid GM medium [3.2 g/l Gamborg's B5 basal medium with minimal organics, 1% (w/v) sucrose, 0.05% (w/v) MES, pH 5.7, and 0.7% (w/v) agar] at 21–23°C under a long-day (LD) photoperiod (16 h light/8 h darkness) with a light intensity of 75–100 µmol/m^2/sec and a relative humidity of 40–50%. Where indicated, agar plates were supplemented with the indicated concentrations of MG132 [(*N*-benzyloxycarbonyl)-leucinyl-leucinyl-leucinal], canavanine, NaCl, mannitol or ABA. The *nac53-1 nac78-1* and *pbe1-2* mutants were used as positive controls for hypersensitivity to proteotoxic and salt or osmotic stress, respectively (Gladman et al., 2016; Han et al., 2019). When required, seedlings were transferred to soil [mixed in a 1:1 ratio with organic Coco Coir planting mixture, supplemented before use with 2 g/l Peters 20-20-20 fertilizer, 80 mg/l $Ca(NO_3)_2$ and 80 mg/l $MgSO_4$] after 2–3 weeks, and grown at 21–23°C under an LD photoperiod.

To generate transgenic plants expressing HA-tagged PBAC5, the genomic region of *PBAC5* encompassing the full coding sequence plus 39-bp upstream of the ATG start codon and 222-bp downstream of the TAA stop codon, which constitute the 5′- and 3′-UTRs, was PCR-amplified from WT Col-0 genomic DNA and recombined into pDONR221 via the Gateway BP clonase II reaction (Thermo Fisher Scientific). Codons for the HA tag (YPYDVPDYA) were then inserted, or the HbYX motif (LYG) deleted, by site-directed mutagenesis using the QuikChange II site-directed mutagenesis kit (Agilent Technologies). The sequence-confirmed *HA–PBAC5* and *HA–PBAC5(ΔHbYX)* clones were recombined into the pMDC99-UBQ10 vector (Curtis and Grossniklaus, 2003; Suttangkakul et al., 2011) via the Gateway LR clonase II reaction (Thermo Fisher Scientific). The plasmids were introduced into *Agrobacterium tumefaciens* strain GV3101 and transformed into homozygous *pbac5-3* plants by the *Agrobacterium*-mediated floral-dip method (Clough and Bent, 1998). F_1 plants resistant to 25 µg/ml hygromycin B were selected and, after a self-cross, double homozygous plants were identified in the F_2 generation by PCR genotyping, immunoblot analysis (see below) and segregation of the F_3 generation on hygromycin-containing medium.

Co-immunoprecipitation of HA–PBAC5

WT and *UBQ10::HA–PBAC5* seedlings were grown for 6 days in 50 ml liquid GM medium (as above, but without agar) and then transferred to fresh medium containing 50 µM MG132 or an equivalent volume of DMSO and incubated for an additional 16 h, with ∼100 mg of dry seeds used per culture, resulting in ∼5 g of fresh weight tissue. Frozen seedlings were ground to a fine powder at liquid N_2 temperatures, and proteins were extracted on ice for 20 min with 1.5 volumes of extraction buffer [50 mM HEPES, pH 7.5, 150 mM NaCl, 10 mM $MgCl_2$, 10% (v/v) glycerol, 5 mM dithiothreitol (DTT), 2 mM phenylmethylsulfonyl fluoride (PMSF), 0.1% (v/v) Triton X-100 and 1× plant protease inhibitor cocktail (Sigma Aldrich, P9599)]. Extracts were filtered through two layers of Miracloth (Calbiochem), clarified at 30,000 ***g*** for 20 min at 4°C, and the resulting supernatants were immediately applied three times at 4°C over a 12 ml PolyPrep chromatography column containing 100 µl (equal to a 50 µl bead volume) of monoclonal anti-HA agarose antibody beads (Sigma-Aldrich, A2095) pre-equilibrated in extraction buffer. The column was washed three times with wash buffer [50 mM HEPES, pH 7.5, 150 mM NaCl, 10 mM $MgCl_2$, 10% (v/v) glycerol and 2 mM DTT], and remaining bound proteins were eluted with 300 µl of 200 mM glycine-HCl (pH 2.5) and immediately neutralized with 60 µl of 1 M Tris-HCl (pH 8.0). Samples of the crude extract, flow through (both diluted 1 in 10), third wash step and elution were analyzed by SDS–PAGE followed by staining for total protein with silver or immunoblotting with appropriate antibodies, as previously described (Gemperline et al., 2019; Marshall et al., 2017). Alternatively, elution fractions were subjected to tandem MS (see below).

Immunological techniques

Frozen *Arabidopsis* seedlings were homogenized in three volumes of protein extraction buffer (50 mM Tris-HCl, pH 7.5, 150 mM NaCl, 2 mM DTT, 1 mM PMSF, 50 mM MG132 and 1× plant protease inhibitor cocktail) and clarified by centrifugation at 16,000 ***g*** for 5 min at 4°C. The supernatant was then mixed with 0.25 volumes of hot 5× SDS–PAGE sample buffer [200 mM Tris-HCl, pH 6.8, 25% (v/v) glycerol, 2% (w/v) SDS, 5% (v/v) 2-mercaptoethanol and 0.1% (w/v) Bromophenol Blue]. The total protein extracts (or elutions from co-immunoprecipitations) were subjected to SDS–PAGE followed by electrophoretic transfer onto Immobilon-P polyvinylidene difluoride (PVDF) membranes (Millipore) for 16 h at 80 mA. Immunoblots were then performed as previously described (Gemperline et al., 2019). Primary antibodies against RPN1 (Yang et al., 2004), RPN3 (Marshall et al., 2015), RPN5, RPN12a, RPT2, PAC1, PBA1, PBF1 (Smalle et al., 2002), RPN10, ubiquitin (van Nocker et al., 1996), RPT4 (Gemperline et al., 2019) and PAG1 (Book et al., 2010) were as previously described (all used at a 1:3000 dilution). Antibodies against 6His (1:1000), FLAG (1:5000), GST (1:5000), HA (1:1000), histone H3 (1:3000) and myc (1:1000) were purchased from BioLegend (906101), Sigma-Aldrich (F1804), Santa Cruz Biotechnology (SC-138), Sigma-Aldrich (H6908), AbCam (AB1791) and BioLegend (908805), respectively.

Yeast two-hybrid assays

Assays for direct protein–protein interactions by Y2H were performed using the ProQuest two-hybrid system (Thermo Fisher Scientific). To clone the *PBAC1–PBAC5* coding sequences, total RNA was first extracted from WT *Arabidopsis* seedlings and converted into cDNA, as described below. Coding sequences amplified by PCR were recombined into pDONR221 via the Gateway BP clonase II reaction. Sequence-confirmed clones were then recombined in-frame with either the Gal4 activation domain or Gal4 DNA-binding domain in the pDEST22 or pDEST32 vectors (Thermo Fisher Scientific), respectively, via the Gateway LR clonase II reaction. Pairwise combinations of coding sequences in pDEST22 and pDEST32 (or the empty vectors as controls) were then co-transformed into yeast strain

MaV203 (Table S5). Cells transformed with both plasmids were selected by growth for 2 days at 30°C on synthetic dropout medium lacking leucine and tryptophan. Protein–protein interactions were then identified by growing for 2 days at 30°C on synthetic dropout medium lacking leucine, tryptophan and histidine, and containing 25 mM 3-amino-1,2,4-triazole (3-AT), with at least four individual colonies tested for each interaction pair. To confirm interactions, single colonies were diluted in sterile H_2O to an OD_{600} of 0.1, and 5 µl were spotted onto both types of selective medium and again grown for 2 days at 30°C.

Bimolecular fluorescence complementation

Sequence-confirmed coding sequences cloned into pDONR221, as above, were recombined in-frame with the N- or C-terminal halves of EYFP in the pSITE-N-EYFP-C1 or pSITE-C-EYFP-C1 vectors (ABRC stock numbers CD3-1648 and CD3-1649, respectively) via Gateway LR clonase II reactions, with expression driven by the cauliflower mosaic virus (CaMV) *35S* promoter. The resulting plasmids were introduced into *A. tumefaciens* strain GV3101, overnight cultures of which were resuspended in 5 ml infiltration buffer [10 mM $MgCl_2$, 10 mM MES, pH 5.7, 100 µM 3′,5′-dimethoxy-4′-hydroxyacetophenone (acetosyringone)], incubated at room temperature for 8–12 h and then used for direct infiltration of 4 to 6-week-old *N. benthamiana* leaves.

Leaf sections ∼2 mm×2 mm were excised 36–48 h after infiltration and visualized by confocal fluorescence microscopy using a Zeiss 510 Meta confocal laser scanning microscope equipped with 20× or 40× oil objectives (numerical apertures 0.75 and 1.30, respectively). Excitation was performed at 488 nm, and emission was collected between 500 and 550 nm. Images were processed using Elements Viewer (Nikon Imaging Software) and/or Adobe Photoshop CC, before conversion to TIFF files for use in the figures. Within each figure, all images (including negative controls) were captured using identical microscope settings, with the exception of bright-field images, where the channel gain was adjusted to provide uniform exposures between images.

Protein purification and *in vitro* pulldown assays

For recombinant protein expression, the *PBAC1*, *PBAC2* and *HA–PBAC5* coding sequences in pDONR221 were recombined into pDEST15, pDEST17 or pDEST14 (Thermo Fisher Scientific), respectively, via the Gateway LR clonase II reaction, resulting in the addition of N-terminal GST, 6His or HA tags, respectively. All proteins were expressed in *E. coli* strain BL21(DE3) pLysS. The cells were cultured at 37°C in 800 ml LB medium to an OD_{600} of 0.6–0.8, followed by a 4-h induction at 30°C with 1 mM isopropyl-β-D-thiogalactopyranoside. Cells were harvested by centrifugation at 4000 *g* for 20 mins at 4°C, frozen in liquid nitrogen, and lysed in two rounds of 10 ml BugBuster Master Mix (EMD Millipore), as according to the manufacturer's instructions.

GST-PBAC1 was affinity purified using GST-Bind Resin (EMD Millipore), as according to the manufacturer's instructions with some minor modifications (Marshall et al., 2015). Briefly, *E. coli* cell lysates were incubated with 2 ml phosphate-buffered saline (PBS)-washed GST-Bind Resin for 1 h at 4°C with continual rotation, then applied to a 30 ml EconoPac chromatography column (Bio-Rad). The beads were washed twice with ice-cold PBS containing 1 M NaCl and once with ice-cold PBS containing 2 M NaCl. Bound proteins were eluted with 10 ml of ice-cold 25 mM MOPS-KOH (pH 7.5) containing 10 mM reduced glutathione (GSH), and the purified proteins were dialyzed overnight at 4°C against 25 mM MOPS-KOH (pH 7.5), before being concentrated 10-fold using an Amicon Ultra-15 centrifugal filter unit with a 10 kDa cut-off limit (Millipore).

6His–PBAC2 was affinity purified using nickel-nitrilotriacetic acid (Ni-NTA) agarose beads (QIAGEN). *E. coli* cell lysates in BugBuster Master Mix containing 10 mM imidazole were applied three times to 1 ml PBS-washed Ni-NTA beads in a 30 ml EconoPac chromatography column at 4°C. After flow-through, the beads were washed once with NaH_2PO_4 wash buffer (50 mM NaH_2PO_4, pH 7.8, 300 mM NaCl and 20 mM imidazole), once with Tris-40 buffer (50 mM Tris-HCl, pH 7.8, 300 mM NaCl and 40 mM imidazole), and once with Tris-60 buffer (50 mM Tris-HCl, pH 7.8, 300 mM NaCl and 60 mM imidazole). Bound proteins were eluted with 5 ml ice-cold elution buffer (50 mM Tris-HCl, pH 7.8, 100 mM NaCl and 300 mM imidazole), and the purified proteins were dialyzed overnight at 4°C to remove the imidazole.

HA–PBAC5 was affinity purified using EZview red anti-HA affinity gel (Sigma-Aldrich). The *E. coli* lysates were incubated with 250 µl PBS-washed anti-HA antibody beads (500 µl of a 50% slurry) for 1 h at 4°C with continual rotation, then applied to a 12 ml PolyPrep chromatography column (Bio-Rad). The beads were then washed three times with PBS containing 1 M NaCl. Bound protein was eluted by incubating the beads for 30 min at 4°C with 300 µl of PBS containing 500 ng/µl of the HA peptide, and the eluant was dialyzed overnight at 4°C against PBS.

To assay direct and indirect interactions between PBAC1, PBAC2 and PBAC5, equal amounts (2 µg) of all three proteins (as determined using a Pierce BCA protein assay kit; Thermo Fisher Scientific) were combined in 500 µl of binding buffer [150 mM Tris-HCl (pH 7.4), 150 mM NaCl, 5 mM $MgCl_2$, 1 mM DTT, 5% (v/v) glycerol and 0.01% (v/v) Triton X-100] and incubated for 2 h at 4°C with continual rotation, before the addition of 100 µl GST-Bind Resin or Ni-NTA agarose beads pre-equilibrated with binding buffer. Samples were incubated for a further 2 h at 4°C with continual rotation, and the beads were then pelleted by centrifugation at 3000 ***g*** for 1 min at 4°C. The beads were washed five times with binding buffer, and bound proteins were eluted into 100 µl of 2× SDS–PAGE sample buffer by heating at 95°C for 5 min. Samples were analyzed by immunoblotting with appropriate antibodies (see above).

Yeast complementation and co-immunoprecipitation assays

Unless otherwise stated, all yeast (*S. cerevisiae*) manipulations were performed according to standard protocols, as described by Marshall et al. (2016). Details of all strains used in this study are given in Table S5. Strain MHY500 (a gift of Mark Hochstrasser, Yale University, New Haven, CT) was used as the WT control. The *Δpba1* and *Δpba2* strains were obtained from the yeast knockout collection (Dharmacon) and cultured on YPDA medium containing 200 µg/ml Geneticin. All genomic deletions were confirmed by PCR genotyping, using the oligonucleotide primer pairs A+B, A+KanB, C+D, KanC+D, and A+D for each deletion strain (Table S4). The *doa5-1* mutation impacting the Doa5/Pup2/α_5 subunit of the CP was described previously (Chen and Hochstrasser, 1996).

For complementation studies, the full-length coding sequences of yeast *PBA1* and *PBA2* were obtained from BY4741 cells by converting RNA isolated by the RNeasy mini kit (QIAGEN) into cDNA, as described below. *Arabidopsis PBAC1*, *PBAC2* and *PBAC5* were amplified from total WT Col-0 cDNA, also generated as described below. The sequences for FLAG, myc or HA tags were incorporated into the appropriate PCR amplification primers. The resulting PCR products were recombined into pDONR221 via the Gateway BP clonase II reaction, and mutations altering the various HbYX and HbF motifs were then introduced by QuikChange II site-directed mutagenesis. The sequence-confirmed clones were recombined into the pAG423-GPD1-ccdB, pAG425-GPD1-ccdB or pAG426-GPD1-ccdB vectors (Addgene, product numbers 14150, 14154, and 14156, respectively) via Gateway LR clonase II reactions. Different plasmid combinations (or the empty vectors as a control) were transformed into the indicated yeast strains using the standard lithium acetate procedure, and transformed cells were cultured on synthetic dropout medium lacking histidine, leucine and/or uracil as required. Cells were then cultured in 15 ml of synthetic dropout medium lacking the auxotrophic markers and, following 16 h overnight growth, diluted to an OD_{600} of 1.0, subjected to a series of 5-fold dilutions, and 5 µl of each dilution was spotted onto solid synthetic dropout medium lacking the auxotrophic markers and containing or lacking 5 µM canavanine. Cells were then grown for 48 h at 30°C prior to imaging.

To assess the *in vivo* interactions between PBAC1, PBAC2 and PBAC5 in yeast, *doa5-1 Δpba1 Δpba2* cells expressing the indicated tagged PBAC protein combinations were grown overnight at 30°C, diluted to an OD_{600} of 0.1 in 15 ml, then grown for an additional 2–3 h until reaching OD_{600} ∼0.5. Cells were harvested by centrifugation at 5000 ***g*** for 1 min, resuspended in 1 ml of IPL buffer [50 mM Tris-HCl, pH 7.5, 150 mM NaCl, 5 mM $MgCl_2$ and 10% (v/v) glycerol, with 20 mM N-ethylmaleimide, 2 mM ATP, 2 mM PMSF, 1 mM benzamidine, 10 µg/ml pepstatin A, 1 µg/ml antipain and 1×

protease inhibitor cocktail (Sigma-Aldrich, P8215) added just before use], lysed by vigorous vortexing at 4°C in the presence of acid-washed glass beads at a volume of ∼50 µl (with five rounds of vortexing for 30 s, then resting on ice for 30 s), and clarified by centrifugation at 16,000 ***g*** for 5 min at 4°C. The supernatant was incubated for 2 h at 4°C with 50 µl of either EZview red anti-HA affinity gel, anti-FLAG M2 affinity gel or EZview red anti-myc affinity gel (Sigma-Aldrich; E6779, A2220 and E6654, respectively) pre-equilibrated in lysis buffer, with continual rotation. The beads were collected by centrifugation at 6000 ***g*** for 5 min at 4°C, washed five times with ice-cold IPL buffer, and bound proteins were eluted in 100 µl SDS–PAGE sample buffer by heating at 95°C for 5 min. Samples were analyzed by immunoblotting with antibodies against FLAG, HA and myc, using immunoblotting with anti-histone H3 antibodies as the negative control.

Reverse transcriptase and quantitative real-time PCR analyses

Total RNA was extracted from 50–100 mg of 7-day-old liquid-grown seedlings using the RNeasy plant mini kit (QIAGEN), as according to the manufacturer's instructions. Following quantification with a NanoDrop 1000 spectrophotometer (Thermo Fisher Scientific), 1 µg of RNA was treated with DNase I (Thermo Fisher Scientific) and converted into cDNA using the SuperScript III first-strand synthesis system (Thermo Fisher Scientific) and oligo$(dT)_{20}$ primers. For standard reverse transcriptase PCR, the cDNA was diluted 1 in 30 following first-strand synthesis, and 5 µl was then amplified in a 20 µl reaction volume also containing 10 µl EconoTaq Plus Green master mix (Lucigen), 3 µl sterile H_2O and 1 µl each of 10 mM forward and reverse primers (Table S4).

Quantitative real-time PCR was performed on three independent biological replicates using a CFX Connect Real-Time System (Bio-Rad) and the LightCycler 480 SYBR Green I master mix (Roche Diagnostics), with three technical replicates for each reaction. In all cases, the amplification factor of the primer pair was experimentally determined to be between 1.90 and 2.10, with the gradient of the standard curve being between −3.59 and −3.10, and the R^2 value being greater than 0.975. For each individual PCR reaction, 5 µl of cDNA (diluted 1 in 30 following first-strand synthesis) was amplified in a 20 µl reaction volume also containing 10 µl SYBR Green I master mix, 3 µl sterile H_2O and 1 µl each of 10 µM forward and reverse primers. Reaction parameters were 95°C for 5 min; 45 cycles of 95°C for 10 s, 55°C for 10 s and 72°C for 30 s; followed by a melting curve program and cooling at 40°C for 2 min. Fluorescence data were collected at the end of each 72°C extension step and continuously during the melting curve program. The relative transcript abundance of target genes was determined using the comparative threshold cycle method (Pfaffl, 2001) using the *ACT2* and *PP2A* reference genes as internal controls (Czechowski et al., 2005). All data was normalized to the WT Col-0 samples.

Proteasome activity assays

Total proteasome activity was assayed as previously described (Marshall et al., 2015), with minor modifications. Seedlings were grown in 5 ml of liquid GM medium at 21–23°C under continuous light for 10 days with gentle shaking (90 rpm). Typically, ∼30 mg of dry seeds was used per culture, resulting in ∼2 g of fresh weight tissue. Frozen tissue was ground to a powder in a mortar and pestle at liquid nitrogen temperatures, and proteins were extracted on ice for 20 min in one volume of extraction buffer [20 mM HEPES-KOH, pH 7.5, 5 mM $MgCl_2$, 10% (v/v) glycerol, 2 mM ATP, 1 mM DTT, 2 mM PMSF, 6 µM chymostatin and 1× plant protease inhibitor cocktail (all from Sigma-Aldrich)]. Extracts were filtered through two layers of Miracloth, clarified at 30,000 ***g*** for 20 min at 4°C, and the supernatant was made 10% (w/v) in PEG 8000 [from an initial stock of 40% (w/v)] and incubated for 30 min at 4°C. The resulting precipitate was collected by centrifugation at 12,000 ***g*** for 15 min at 4°C and resuspended in 500 µl of extraction buffer, a step that has been shown to remove the majority of lower molecular weight proteases that might interfere with the assay (Yang et al., 2004). The total protein concentration of each sample was determined using a Pierce BCA protein assay kit, and an equal mass of protein (10 µg) from each sample was assayed for proteasome activity in the presence or absence of 80 µM MG132 (Kisselev and Goldberg, 2005). Protein samples in a volume of 20 µl were incubated for 20 min at 37°C in 1 ml of assay buffer (50 mM Tris-HCl, pH 7.0, 2 mM $MgCl_2$, 1 mM ATP and 2 mM 2-mercaptoethanol) containing 100 µM of the fluorogenic substrate N-succinyl-leucyl-leucyl-valyl-tyrosyl-7-amino-4-methylcoumarin (succinyl-LLVY-AMC; Sigma-Aldrich). Reactions were quenched by the addition of 1 ml of 80 mM sodium acetate (pH 4.3), and the fluorescence of released AMC was monitored using a TKO 100 fluorometer (Hoefer Scientific Instruments), with an excitation wavelength of 365 nm and an emission wavelength of 460 nm. Three technical replicates were assayed for each sample; the data from three biological replicates were averaged and normalized to the activity observed in WT Col-0 tissue in the absence of MG132.

Glycerol gradient centrifugation

Glycerol gradient fractionation of 26S proteasome subcomplexes was performed essentially as previously described (Gemperline et al., 2019). Seedlings were grown as above and proteins were extracted in one volume of extraction buffer [20 mM HEPES-KOH, pH 7.5, 5 mM $MgCl_2$, 10% (v/v) glycerol, 2 mM ATP, 1 mM DTT, 2 mM PMSF, 6 µM chymostatin, 1× plant protease inhibitor cocktail, 10 mM phosphocreatine and 1 mg/ml creatine phosphokinase (all from Sigma-Aldrich)]. Extracts were filtered through two layers of Miracloth, clarified at 30,000 ***g*** for 20 min at 4°C, and 1 ml of supernatant was loaded onto an 11 ml, 10–40% (v/v) glycerol density gradient in extraction buffer, made using an Auto-DensiFlow density gradient fractionator (Labconco). Following centrifugation at 100,000 ***g*** for 18 h at 4°C, 500 µl fractions were manually collected with a Gilson-type P1000 pipette, and 10 µl of each fraction was subjected to immunoblot analysis as described above.

Tandem mass spectrometry

Samples from three independent anti-HA immunoprecipitation experiments were subjected to tandem MS as previously described (Marshall et al., 2019), with minor modifications. Briefly, eluants were vacuum dried and denatured in 300 µl of 8 M urea, 25 mM $(NH_4)HCO_3$. Proteins were then reduced with 10 mM DTT at room temperature for 1 h and alkylated in the dark in the presence of 50 mM 2-chloroacetamide at room temperature for a further 1 h. Excess alkylating agent was quenched with 50 mM DTT for 5 min at room temperature, and samples were diluted with 1.2 ml of 25 mM $(NH_4)HCO_3$ to reduce the urea concentration to below 1.5 M. Proteolytic digestion was initiated by incubating the samples with 1 µg of sequencing-grade modified porcine trypsin (Promega) for 18 h at 37°C. Resulting peptides were vacuum dried to a final volume of ∼300 µl, acidified with 10% (v/v) trifluoroacetic acid (TFA) until the pH was less than 3.0, and desalted and concentrated on a 100 µl Bond Elut OMIX C18 pipette tip (Agilent Technologies), as according to the manufacturer's instructions. Peptides were eluted in 50 µl of 75% (v/v) acetonitrile, 0.1% (v/v) acetic acid, then lyophilized and resuspended in 17 µl 5% (v/v) acetonitrile, 0.1% (v/v) formic acid.

Nano-scale ultra-high-performance liquid chromatographic (UHPLC) separation of tryptic peptides was performed on a Dionex Ultimate 3000 Rapid Separation LC system (Thermo Fisher Scientific) with a C18 analytical column [Acclaim PepMap RSLC C18 column, 2 µm particle size, 100 Å pore size, 75 µm×25 cm (Thermo Fisher Scientific)] by the application of a linear 2 h gradient from 4.0% to 36.0% (v/v) acetonitrile in 0.1% (v/v) formic acid, with the column flow rate set to 250 nl/min. MS analysis of the eluted tryptic peptides was performed online using a Q Exactive Plus mass spectrometer (Thermo Fisher Scientific) possessing a Nanospray Flex ion source (Thermo Fisher Scientific) fitted with a stainless steel nano-bore emitter operated in positive electrospray ionization (ESI) mode at a capillary voltage of 1.9 kV. Data-dependent acquisition of full MS scans within a mass range of 380–1500 m/*z* was performed at a resolution of 70,000, with the automatic gain control (AGC) target set to 3.0×10^6 ion intensity and the maximum fill time set to 200 ms. High energy collision-induced dissociation (HCD) fragmentation of the top 15 most intense peaks was performed with a normalized collision energy of 28, an intensity threshold of 4×10^4 counts and an isolation window of 3.0 m/*z*, excluding precursors that had unassigned, +1, +7 or +8 charge states. MS/MS scans were acquired at a resolution of 17,500, with an AGC target of 2×10^5 and a maximum fill time of 100 ms. All peaks were recorded in profile mode.

Dynamic exclusion was performed with a repeat count of two and an exclusion duration of 30 s, while the minimum MS ion count for triggering MS/MS was set to 4.0×10^3 counts.

The resulting MS/MS spectral files were processed using Proteome Discoverer (version 2.0.0.802; Thermo Fisher Scientific), set up to interrogate the *A. thaliana* Col-0 proteome file TAIR10_pep_20101214_updated.fasta (available at the Arabidopsis Information Resource; www.arabidopsis.org/). Peptides were assigned using SEQUEST HT (Eng et al., 1994), with search parameters set to assume the digestion enzyme trypsin with a maximum of one missed cleavage, a minimum peptide length of six, precursor mass tolerances of 10 ppm, and fragment mass tolerances of 0.02 Da. Carbamidomethylation of cysteine was specified as a static modification, whereas oxidation of methionine and N-terminal acetylation were specified as dynamic modifications. A target false discovery rate (FDR) was determined using the Protein FDR Validator node, where all proteins with a q-value higher than 0.01 (strict, high confidence) and 0.05 (relaxed, medium confidence) were included in the analysis. Proteins that contained similar peptides, and which could not be differentiated based on the MS/MS analysis alone, were grouped to satisfy the principles of parsimony. Peptide abundances were quantified from the precursor ion intensities available in the MS1 scans, with the relative abundances for the full-length proteins being generated from the averages of three biological replicates, each analysed in duplicate.

Label-free MS1 quantification was performed as previously described (Silva et al., 2006) using Proteome Discoverer with a minimum Quan value threshold set to 0.0001 using unique peptides, and '3 Top N' peptides used for area calculation. The resulting values were $\log_2$-transformed and missing values were imputed assuming a normal distribution, width distribution shrinkage of 0.3 and a downshift of 1.8 standard deviations using the Perseus computational platform (Tyanova et al., 2016). Significant changes in protein abundance were calculated in Perseus by analysis of variance (ANOVA) contrasts (P-value <0.05; FDR <1%; S0=2), allowing 250 permutations. Details of all quantification data are provided in Table S6.

Statistical analyses

Details of MS-based statistical analyses are provided above. All other datasets were statistically analyzed using one-way ANOVA followed by Tukey's post hoc tests to identify significantly different data points. At least three biological replicates were performed in all cases, unless otherwise indicated in the figure legend.

Accession numbers

All accession numbers for genes and proteins used in this study are given in Table S1.

Acknowledgements

We thank Mark Hochstrasser for sharing yeast strains, and Erin Gemperline, Nicholas P. Gladman, Weiming Hu, and Joseph M. Walker for advice and technical support.

Competing interests

The authors declare no competing or financial interests.

Author contributions

Conceptualization: R.S.M., D.C.G., A.J.B., R.D.V.; Methodology: R.S.M., D.C.G., F.M., A.J.B., K.H.; Validation: R.S.M., D.C.G., F.M., A.J.B., K.H.; Formal analysis: R.S.M., D.C.G., F.M., A.J.B., K.H., R.D.V.; Investigation: D.C.G., A.J.B., K.H.; Data curation: R.S.M., D.C.G., F.M., K.H.; Writing - original draft: R.S.M., R.D.V.; Writing - review & editing: R.S.M., D.C.G., F.M., K.H., R.D.V.; Visualization: D.C.G., F.M., K.H., R.D.V.; Supervision: R.D.V.; Project administration: R.D.V.; Funding acquisition: R.D.V.

Funding

This work was supported by grants from the National Institutes of Health – National Institute of General Medical Science (R01-GM124452) and the National Science Foundation – Plant Genome Research Program (IOS-1339325) to R.D.V., plus a graduate fellowship from the University of Wisconsin Genetics Training Program sponsored by the National Institutes of Health to D.C.G. Deposited in PMC for release after 12 months.

Data availability

The MS-based proteomics data have been deposited to the ProteomeXchange Consortium (http://www.proteomexchange.org/) via the PRIDE partner repository with the dataset identifier PXD018717.

Supplementary Information

Supplementary information is available online at https://jcs.biologists.org/lookup/doi/10.1242/jcs.249862.supplemental

Peer review history

The peer review history is available online at https://jcs.biologists.org/lookup/doi/10.1242/jcs.249862.reviewer-comments.pdf

References

Ahuja, J. S., Sandhu, R., Mainpal, R., Lawson, C., Henley, H., Hunt, P. A., Yanowitz, J. L. and Börner, G. V. (2017). Control of meiotic pairing and recombination by chromosomally tethered 26S proteasome. *Science* **355**, 408-411. doi:10.1126/science.aaf4778

Albalat, R. and Cañestro, C. (2016). Evolution by gene loss. *Nat. Rev. Genet.* **17**, 379-391. doi:10.1038/nrg.2016.39

Arendt, C. S. and Hochstrasser, M. (1997). Identification of the yeast 20S proteasome catalytic centers and subunit interactions required for active-site formation. *Proc. Natl. Acad. Sci. USA* **94**, 7156-7161. doi:10.1073/pnas.94.14.7156

Bhattacharyya, S., Yu, H., Mim, C. and Matouschek, A. (2014). Regulated protein turnover: snapshots of the proteasome in action. *Nat. Rev. Mol. Cell Biol.* **15**, 122-133. doi:10.1038/nrm3741

Book, A. J., Gladman, N. P., Lee, S. S., Scalf, M., Smith, L. M. and Vierstra, R. D. (2010). Affinity purification of the *Arabidopsis* 26 S proteasome reveals a diverse array of plant proteolytic complexes. *J. Biol. Chem.* **285**, 25554-25569. doi:10.1074/jbc.M110.136622

Brinkmann, K., Schell, M., Hoppe, T. and Kashkar, H. (2015). Regulation of the DNA damage response by ubiquitin conjugation. *Front. Genet.* **6**, 98. doi:10.3389/fgene.2015.00098

Bucher, P., Karplus, K., Moeri, N. and Hofmann, K. (1996). A flexible motif search technique based on generalized profiles. *Comp. Chem.* **20**, 3-23. doi:10.1016/S0097-8485(96)80003-9

Burri, L., Höckendorff, J., Boehm, U., Klamp, T., Dohmen, R. J. and Lévy, F. (2000). Identification and characterization of a mammalian protein interacting with 20S proteasome precursors. *Proc. Natl. Acad. Sci. USA* **97**, 10348-10353. doi:10.1073/pnas.190268597

Chen, P. and Hochstrasser, M. (1996). Autocatalytic subunit processing couples active site formation in the 20S proteasome to completion of assembly. *Cell* **86**, 961-972. doi:10.1016/S0092-8674(00)80171-3

Clough, S. J. and Bent, A. F. (1998). Floral dip: a simplified method for *Agrobacterium*-mediated transformation of *Arabidopsis thaliana*. *Plant J.* **16**, 735-743. doi:10.1046/j.1365-313x.1998.00343.x

Curtis, M. D. and Grossniklaus, U. (2003). A Gateway cloning vector set for high-throughput functional analysis of genes *in planta*. *Plant Physiol.* **133**, 462-469. doi:10.1104/pp.103.027979

Czechowski, T., Stitt, M., Altmann, T., Udvardi, M. K. and Scheible, W. R. (2005). Genome-wide identification and testing of superior reference genes for transcript normalization in *Arabidopsis*. *Plant Physiol.* **139**, 5-17. doi:10.1104/pp.105.063743

Dudler, R. (2013). Manipulation of host proteasomes as a virulence mechanism of plant pathogens. *Annu. Rev. Phytopathol.* **51**, 521-542. doi:10.1146/annurev-phyto-082712-102312

Eng, J. K., McCormack, A. L. and Yates, J. R. (1994). An approach to correlate tandem mass spectral data of peptides with amino acid sequences in a protein database. *J. Am. Soc. Mass Spectrom.* **5**, 976-989. doi:10.1016/1044-0305(94)80016-2

Finley, D. and Prado, M. A. (2020). The proteasome and its network: engineering for adaptability. *Cold Spring Harb. Perspect. Biol.* **12**, a033985. doi:10.1101/cshperspect.a033985

Finley, D., Ulrich, H. D., Sommer, T. and Kaiser, P. (2012). The ubiquitin-proteasome system of *Saccharomyces cerevisiae*. *Genetics* **192**, 319-360. doi:10.1534/genetics.112.140467

Gemperline, D. C., Marshall, R. S., Lee, K.-H., Zhao, Q., Hu, W., McLoughlin, F., Scalf, M., Smith, L. M. and Vierstra, R. D. (2019). Proteomic analysis of affinity-purified 26S proteasomes identifies a suite of assembly chaperones in *Arabidopsis*. *J. Biol. Chem.* **294**, 17570-17592. doi:10.1074/jbc.RA119.010219

Gille, C., Goede, A., Schlöetelburg, C., Preissner, R., Kloetzel, P. M., Göbel, U. B. and Frömmel, C. (2003). A comprehensive view on proteasomal sequences: implications for the evolution of the proteasome. *J. Mol. Biol.* **326**, 1437-1448. doi:10.1016/S0022-2836(02)01470-5

Gladman, N. P., Marshall, R. S., Lee, K.-H. and Vierstra, R. D. (2016). The proteasome stress regulon is controlled by a pair of NAC transcription factors in *Arabidopsis*. *Plant Cell* **28**, 1279-1296. doi:10.1105/tpc.15.01022

Greene, E. R., Dong, K. C. and Martin, A. (2020). Understanding the 26S proteasome molecular machine from a structural and conformational dynamics perspective. *Curr. Opin. Struct. Biol.* **61**, 33-41. doi:10.1016/j.sbi.2019.10.004
Groll, M., Bajorek, M., Köhler, A., Moroder, L., Rubin, D. M., Huber, R., Glickman, M. H. and Finley, D. (2000). A gated channel into the proteasome core particle. *Nat. Struct. Biol.* **7**, 1062-1067. doi:10.1038/80992
Guan, H., Wang, Y., Yu, T., Huang, Y., Li, M., Saeed, A. F., Perčulija, V., Li, D., Xiao, J., Wang, D. et al. (2020). Cryo-EM structures of the human PA200 and PA200-20S complex reveal regulation of proteasome gate opening and two PA200 apertures. *PLoS Biol.* **18**, 3000654. doi:10.1371/journal.pbio.3000654
Guijarro-Clarke, C., Holland, P. W. H. and Paps, J. (2020). Widespread patterns of gene loss in the evolution of the animal kingdom. *Nat. Ecol. Evol.* **4**, 519-523. doi:10.1038/s41559-020-1129-2
Hammack, L. J., Panfair, D. and Kusmierczyk, A. R. (2020). A novel proteasome assembly intermediate bypasses the need to form α-rings first. *Biochem. Biophys. Res. Commun.* **525**, 107-112. doi:10.1016/j.bbrc.2020.02.044
Han, J. J., Yang, X., Wang, Q., Tang, L., Yu, F., Huang, X., Wang, Y., Liu, J. X. and Xie, Q. (2019). The β_5 subunit is essential for intact 26S proteasome assembly to specifically promote plant autotrophic growth under salt stress. *New Phytol.* **221**, 1359-1368. doi:10.1111/nph.15471
Heinemeyer, W., Fischer, M., Krimmer, T., Stachon, U. and Wolf, D. H. (1997). The active sites of the eukaryotic 20 S proteasome and their involvement in subunit precursor processing. *J. Biol. Chem.* **272**, 25200-25209. doi:10.1074/jbc.272.40.25200
Higuchi-Sanabria, R., Frankino, P. A., Paul, J. W., Tronnes, S. U. and Dillin, A. (2018). A futile battle: protein quality control and the stress of ageing. *Dev. Cell* **44**, 139-163. doi:10.1016/j.devcel.2017.12.020
Hirano, Y., Hendil, K. B., Yashiroda, H., Iemura, S., Nagane, R., Hioki, Y., Natsume, T., Tanaka, K. and Murata, S. (2005). A heterodimeric complex that promotes the assembly of mammalian 20S proteasomes. *Nature* **437**, 1381-1385. doi:10.1038/nature04106
Hirano, Y., Hayashi, H., Iemura, S., Hendil, K. B., Niwa, S., Kishimoto, T., Kasahara, M., Natsume, T., Tanaka, K. and Murata, S. (2006). Co-operation of multiple chaperones required for the assembly of mammalian 20S proteasomes. *Mol. Cell* **24**, 977-984. doi:10.1016/j.molcel.2006.11.015
Hirano, Y., Kaneko, T., Okamoto, K., Bai, M., Yashiroda, H., Furuyama, K., Kato, K., Tanaka, K. and Murata, S. (2008). Dissecting the β-ring assembly pathway of the mammalian 20S proteasome. *EMBO J.* **27**, 2204-2213. doi:10.1038/emboj.2008.148
Howell, L. A., Tomko, R. J. and Kusmierczyk, A. R. (2017). Putting it all together: intrinsic and extrinsic mechanisms governing proteasome biogenesis. *Front. Biol.* **12**, 19-48. doi:10.1007/s11515-017-1439-1
Howell, L. A., Peterson, A. K. and Tomko, R. J. (2019). Proteasome subunit α_1 over-expression preferentially drives canonical proteasome biogenesis and enhances stress tolerance in yeast. *Sci. Rep.* **9**, 12418. doi:10.1038/s41598-019-48889-5
Katoh, K., Misawa, K., Kuma, K. and Miyata, T. (2002). MAFFT: a novel method for rapid multiple sequence alignment based on fast Fourier transform. *Nucleic Acids Res.* **30**, 3059-3066. doi:10.1093/nar/gkf436
Kisselev, A. F. and Goldberg, A. L. (2005). Monitoring activity and inhibition of 26S proteasomes with fluorogenic peptide substrates. *Methods Enzymol.* **398**, 364-378. doi:10.1016/S0076-6879(05)98030-0
Klepikova, A. V., Kasianov, A. S., Gerasimov, E. S., Logacheva, M. D. and Penin, A. A. (2016). A high resolution map of the *Arabidopsis thaliana* developmental transcriptome based on RNA-seq profiling. *Plant J.* **88**, 1058-1070. doi:10.1111/tpj.13312
Kock, M., Nunes, M. M., Hemann, M., Kube, S., Dohmen, R. J., Herzog, F., Ramos, P. C. and Wendler, P. (2015). Proteasome assembly from 15S precursors involves major conformational changes and recycling of the Pba1-Pba2 chaperone. *Nat. Commun.* **6**, 6123. doi:10.1038/ncomms7123
Köhler, A., Cascio, P., Leggett, D. S., Woo, K. M., Goldberg, A. L. and Finley, D. (2001). The axial channel of the proteasome core particle is gated by the Rpt2 ATPase and controls both substrate entry and product release. *Mol. Cell* **7**, 1143-1152. doi:10.1016/S1097-2765(01)00274-X
Kusmierczyk, A. R., Kunjappu, M. J., Funakoshi, M. and Hochstrasser, M. (2008). A multimeric assembly factor controls the formation of alternative 20S proteasomes. *Nat. Struct. Mol. Biol.* **15**, 237-244. doi:10.1038/nsmb.1389
Kusmierczyk, A. R., Kunjappu, M. J., Kim, R. Y. and Hochstrasser, M. (2011). A conserved 20S proteasome assembly factor requires a C-terminal HbYX motif for proteasomal precursor binding. *Nat. Struct. Mol. Biol.* **18**, 622-629. doi:10.1038/nsmb.2027
Le Tallec, B., Barrault, M.-B., Courbeyrette, R., Guérois, R., Marsolier-Kergoat, M.-C. and Peyroche, A. (2007). 20S proteasome assembly is orchestrated by two distinct pairs of chaperones in yeast and mammals. *Mol. Cell* **27**, 660-674. doi:10.1016/j.molcel.2007.06.025
Lee, K. H., Minami, A., Marshall, R. S., Book, A. J., Farmer, L. M., Walker, J. M. and Vierstra, R. D. (2011). The RPT2 subunit of the 26S proteasome directs complex assembly, histone dynamics, and gametophyte and sporophyte development in *Arabidopsis*. *Plant Cell* **23**, 4298-4317. doi:10.1105/tpc.111.089482
Li, X., Kusmierczyk, A. R., Wong, P., Emili, A. and Hochstrasser, M. (2007). β-subunit appendages promote 20S proteasome assembly by overcoming an Ump1-dependent checkpoint. *EMBO J.* **26**, 2339-2349. doi:10.1038/sj.emboj.7601681
Love, M. I., Huber, W. and Anders, S. (2014). Moderated estimation of fold change and dispersion for RNA-seq data with DESeq2. *Genome Biol.* **15**, 550. doi:10.1186/s13059-014-0550-8
Majumder, P. and Baumeister, W. (2019). Proteasomes: unfoldase-assisted protein degradation machines. *Biol. Chem.* **401**, 183-199. doi:10.1515/hsz-2019-0344
Majumder, P., Rudack, T., Beck, F., Danev, R., Pfeifer, G., Nagy, I. and Baumeister, W. (2019). Cryo-EM structures of the archaeal PAN-proteasome reveal an around-the-ring ATPase cycle. *Proc. Natl. Acad. Sci. USA* **116**, 534-539. doi:10.1073/pnas.1817752116
Marshall, R. S. and Vierstra, R. D. (2019). Dynamic regulation of the 26S proteasome: from synthesis to degradation. *Front. Mol. Biosci.* **6**, 40. doi:10.3389/fmolb.2019.00040
Marshall, R. S., Li, F., Gemperline, D. C., Book, A. J. and Vierstra, R. D. (2015). Autophagic degradation of the 26S proteasome is mediated by the dual ATG8/ubiquitin receptor RPN10 in *Arabidopsis*. *Mol. Cell* **58**, 1053-1066. doi:10.1016/j.molcel.2015.04.023
Marshall, R. S., McLoughlin, F. and Vierstra, R. D. (2016). Autophagic turnover of inactive 26S proteasomes in yeast is directed by the ubiquitin receptor Cue5 and the Hsp42 chaperone. *Cell Rep.* **16**, 1717-1732. doi:10.1016/j.celrep.2016.07.015
Marshall, R. S., Gemperline, D. C. and Vierstra, R. D. (2017). Purification of 26S proteasomes and their subcomplexes from plants. *Methods Mol. Biol.* **1511**, 301-334. doi:10.1007/978-1-4939-6533-5_24
Marshall, R. S., Hua, Z., Mali, S., McLoughlin, F. and Vierstra, R. D. (2019). ATG8-binding UIM proteins define a new class of autophagy adaptors and receptors. *Cell* **177**, 766-781. doi:10.1016/j.cell.2019.02.009
Padmanabhan, A., Vuong, S. A.-T. and Hochstrasser, M. (2016). Assembly of an evolutionarily conserved alternative proteasome isoform in human cells. *Cell Rep.* **14**, 2962-2974. doi:10.1016/j.celrep.2016.02.068
Panfair, D., Ramamurthy, A. and Kusmierczyk, A. R. (2015). An α-ring independent assembly pathway for the 20S proteasome. *Sci. Rep.* **5**, 13130. doi:10.1038/srep13130
Pfaffl, M. W. (2001). A new mathematical model for relative quantification in real-time RT-PCR. *Nucleic Acids Res.* **29**, 45. doi:10.1093/nar/29.9.e45
Pilla, E., Schneider, K. and Bertolotti, A. (2017). Coping with protein quality control failure. *Annu. Rev. Cell Dev. Biol.* **33**, 439-465. doi:10.1146/annurev-cellbio-111315-125334
Pohl, C. and Dikic, I. (2019). Cellular quality control by the ubiquitin-proteasome system and autophagy. *Science* **366**, 818-822. doi:10.1126/science.aax3769
Rabl, J., Smith, D. M., Yu, Y., Chang, S. C., Goldberg, A. L. and Cheng, Y. (2008). Mechanism of gate opening in the 20S proteasome by the proteasomal ATPases. *Mol. Cell* **30**, 360-368. doi:10.1016/j.molcel.2008.03.004
Ramachandran, K. V., Fu, J. M., Schaffer, T. B., Na, C. H., Delannoy, M. and Margolis, S. S. (2018). Activity-dependent degradation of the nascentome by the neuronal membrane proteasome. *Mol. Cell* **71**, 169-177.e6. doi:10.1016/j.molcel.2018.06.013
Ramos, P. C., Höckendorff, J., Johnson, E. S., Varshavsky, A. and Dohmen, R. J. (1998). Ump1p is required for proper maturation of the 20S proteasome and becomes its substrate upon completion of assembly. *Cell* **92**, 489-499. doi:10.1016/S0092-8674(00)80942-3
Rape, M. (2018). Ubiquitylation at the crossroads of development and disease. *Nat. Rev. Mol. Cell Biol.* **19**, 59-70. doi:10.1038/nrm.2017.83
Ronquist, F. and Huelsenbeck, J. P. (2003). MrBayes 3: bayesian phylogenetic inference under mixed models. *Bioinformatics* **19**, 1572-1574. doi:10.1093/bioinformatics/btg180
Rousseau, A. and Bertolotti, A. (2018). Regulation of proteasome assembly and activity in health and disease. *Nat. Rev. Mol. Cell Biol.* **19**, 697-712. doi:10.1038/s41580-018-0040-z
Saitou, N. and Nei, M. (1987). The neighbor-joining method: a new method for reconstructing phylogenetic trees. *Mol. Biol. Evol.* **4**, 406-425.
Seemüller, E., Lupas, A., Stock, D., Löwe, J., Huber, R. and Baumeister, W. (1995). The proteasome from *Thermoplasma acidophilum*: a threonine protease. *Science* **268**, 579-582. doi:10.1126/science.7725107
Silva, J. C., Gorenstein, M. V., Li, G. Z., Vissers, J. P. and Geromanos, S. J. (2006). Absolute quantification of proteins by LCMSE: a virtue of parallel MS acquisition. *Mol. Cell. Proteomics* **5**, 144-156. doi:10.1074/mcp.M500230-MCP200
Smalle, J., Kurepa, J., Yang, P., Babiychuk, E., Kushnir, S., Durski, A. M. and Vierstra, R. D. (2002). Cytokinin growth responses in *Arabidopsis* involve the 26S proteasome subunit RPN12. *Plant Cell* **14**, 17-32. doi:10.1105/tpc.010381
Smith, D. M., Chang, S. C., Park, S., Finley, D., Cheng, Y. and Goldberg, A. L. (2007). Docking of the C-termini of the proteasomal ATPases into the 20S proteasome α-ring opens the gate for substrate entry. *Mol. Cell* **27**, 731-744. doi:10.1016/j.molcel.2007.06.033

Söding, J. (2005). Protein homology detection by HMM-HMM comparison. *Bioinformatics* **21**, 951-960. doi:10.1093/bioinformatics/bti125

Stadtmueller, B. M., Kish-Trier, E., Ferrell, K., Petersen, C. N., Robinson, H., Myszka, D. G., Eckert, D. M., Formosa, T. and Hill, C. P. (2012). Structure of a proteasome Pba1-Pba2 complex: implications for proteasome assembly, activation and biological function. *J. Biol. Chem.* **287**, 37371-37382. doi:10.1074/jbc.M112.367003

Suttangkakul, A., Li, F., Chung, T. and Vierstra, R. D. (2011). The ATG1/ATG13 protein kinase complex is both a regulator and a target of autophagic recycling in *Arabidopsis*. *Plant Cell* **23**, 3761-3779. doi:10.1105/tpc.111.090993

Takagi, K., Saeki, Y., Yashiroda, H., Yagi, H., Kaiho, A., Murata, S., Yamane, T., Tanaka, K., Mizushima, T. and Kato, K. (2014). Pba3-Pba4 heterodimer acts as a molecular matchmaker in proteasome α-ring formation. *Biochem. Biophys. Res. Commun.* **450**, 1110-1114. doi:10.1016/j.bbrc.2014.06.119

Tian, G., Park, S., Lee, M. J., Huck, B., McAllister, F., Hill, C. P., Gygi, S. P. and Finley, D. (2011). An asymmetric interface between the regulatory and core particles of the proteasome. *Nat. Struct. Mol. Biol.* **18**, 1259-1267. doi:10.1038/nsmb.2147

Tyanova, S., Temu, T., Sinitcyn, P., Carlson, A., Hein, M. Y., Geiger, T., Mann, M. and Cox, J. (2016). The Perseus computational platform for comprehensive analysis of (prote)omics data. *Nat. Methods* **13**, 731-740. doi:10.1038/nmeth.3901

Üstün, S., Hafrén, A., Liu, Q., Marshall, R. S., Minina, E. A., Bozhkov, P. V., Vierstra, R. D. and Hofius, D. (2018). Bacteria exploit autophagy for proteasome degradation and enhanced virulence in plants. *Plant Cell* **30**, 668-685. doi:10.1105/tpc.17.00815

van Nocker, S., Deveraux, Q., Rechsteiner, M. and Vierstra, R. D. (1996). *Arabidopsis MBP1* gene encodes a conserved ubiquitin recognition component of the 26S proteasome. *Proc. Natl. Acad. Sci. USA* **93**, 856-860. doi:10.1073/pnas.93.2.856

Yu, Z., Kleifeld, O., Lande-Atir, A., Bsoul, M., Kleiman, M., Krutauz, D., Book, A., Vierstra, R. D., Hofmann, K., Reis, N. et al. (2011). Dual function of Rpn5 in two PCI complexes, the 26S proteasome and COP9 signalosome. *Mol. Biol. Cell* **22**, 911-920. doi:10.1091/mbc.e10-08-0655

Wang, G., Fan, W., Ou, M., Wang, X., Qin, H., Feng, F., Du, Y., Ni, J., Tang, J., Song, R. et al. (2019). *Dek40* encodes a PBAC4 protein required for 20S proteasome biogenesis and seed development. *Plant Physiol.* **180**, 2120-2132. doi:10.1104/pp.18.01419

Wani, P. S., Rowland, M. A., Ondracek, A., Deeds, E. J. and Roelofs, J. (2015). Maturation of the proteasome core particle induces an affinity switch that controls regulatory particle association. *Nat. Commun.* **6**, 6384. doi:10.1038/ncomms7384

Wu, W., Sahara, K., Hirayama, S., Zhao, X., Watanabe, A., Hamazaki, J., Yashiroda, H. and Murata, S. (2018). PAC1-PAC2 proteasome assembly chaperone retains the core α_4-α_7 assembly intermediates in the cytoplasm. *Genes Cells* **23**, 839-848. doi:10.1111/gtc.12631

Xu, F.-Q. and Xue, H.-W. (2019). The ubiquitin-proteasome system in plant responses to environments. *Plant Cell Environ.* **42**, 2931-2944. doi:10.1111/pce.13633

Yang, P., Fu, H., Walker, J. M., Papa, C. M., Smalle, J., Ju, Y. M. and Vierstra, R. D. (2004). Purification of the *Arabidopsis* 26 S proteasome: biochemical and molecular analyses revealed the presence of multiple isoforms. *J. Biol. Chem.* **279**, 6401-6413. doi:10.1074/jbc.M311977200

Yashiroda, H., Mizushima, T., Okamoto, K., Kameyama, T., Hayashi, H., Kishimoto, T., Niwa, S., Kasahara, M., Kurimoto, E., Sakata, E. et al. (2008). Crystal structure of a chaperone complex that contributes to the assembly of yeast 20S proteasomes. *Nat. Struct. Mol. Biol.* **15**, 228-236. doi:10.1038/nsmb.1386

Zheng, N. and Shabek, N. (2017). Ubiquitin ligases: structure, function, and regulation. *Annu. Rev. Biochem.* **86**, 129-157. doi:10.1146/annurev-biochem-060815-014922